Article
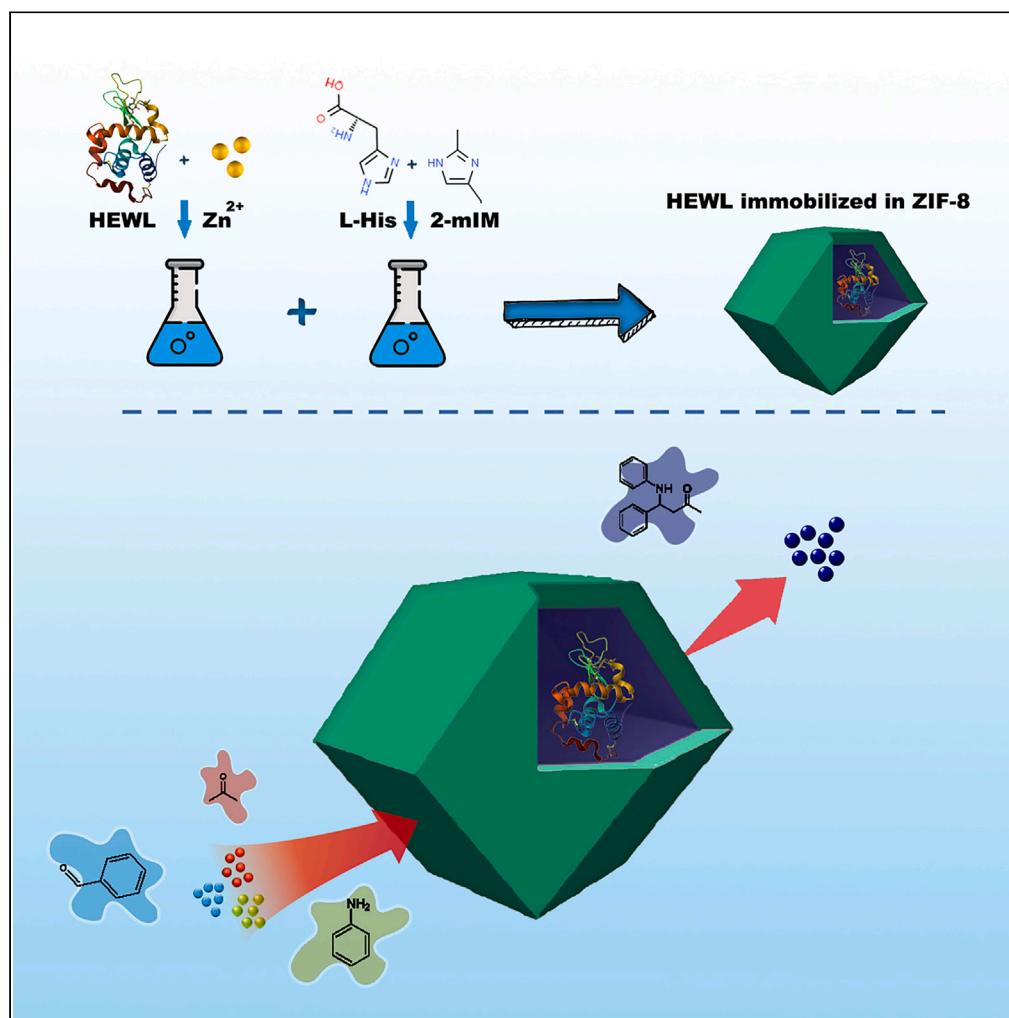
Hen egg white lysozyme encapsulated in ZIF-8 for performing promiscuous enzymatic Mannich reaction

Hamid R. Kalhor,
Zeinab Piraman,
Yasaman Fathali

kalhor@sharif.edu

Highlights

Promiscuous synthesis of Mannich products by hen egg white lysozyme

Immobilization of lysozyme in zeolitic imidazolate framework-8, enhancing the reaction

Studying the mutant (D52A) lysozyme in performing Mannich reaction

Mechanistic studies in the lysozyme Mannich reaction by computational methods

Article

Hen egg white lysozyme encapsulated in ZIF-8 for performing promiscuous enzymatic Mannich reaction

Hamid R. Kalhor,[1,2,*] Zeinab Piraman,[1] and Yasaman Fathali[1]

SUMMARY

Hen egg white lysozyme (HEWL) was exploited for the synthesis of β-amino carbonyl compounds through a direct and three-component Mannich reaction in aqueous, confirming high chemoselectivity toward imine. In order to further extend the applications of the enzyme, HEWL was encapsulated using a metal-organic framework (MOF). The reactivity, stereoselectivity, and reusability of the encapsulated enzyme were investigated. The reaction was significantly enhanced as compared to the non-encapsulated enzyme. A mutated version of the enzyme, containing Asp52Ala (D52A), lacking important catalytical residue, has lost the bacterial site activity against *Micrococcus luteus* (*M. luteus*) while the D52A variant displayed an increased rate of the Mannich reaction, indicating a different catalytical residue involved in the promiscuous reaction. Based on site-directed mutagenesis, molecular docking, and molecular dynamic studies, it was proposed that π-stacking, H-bond interactions, and the presence of water in the active site may play crucial roles in the mechanism of the reaction.

INTRODUCTION

In the last few decades, eco-friendly solvents have gained more interest in the field of green chemistry with the development of aqueous catalysis.[1–3] Exploiting enzymes in organic synthesis has expanded rapidly due to their green and environmental-friendly approach to perform chemical reactions with high selectivity, mild reaction conditions (e.g., low temperature and neutral pH), and broad substrate specificity.[4–6] Catalytic promiscuity, by one of its definitions, is the ability of an enzyme to catalyze its natural reaction, along with one or more alternative reactions of non-natural substrates.[7,8] In many respects, hydrolases are a more commonly used class of enzymes in carbon-carbon bond formation.[9] To date, several enzymes belonging to the hydrolase family (EC 3.2) have been used for C-C bond formation in organic synthesis, including *Candida cylindracea* (CcL) lipase,[10] *Candida Antarctica* lipase B (CAL-B),[11] *Porcine Pancreas Lipase* (PPL),[12,13] *porcine pepsin*,[14] *Bovine Pancreatic Lipase* (BPL),[15] *D-aminoacylase*,[16,17] *nuclease p1 from Penicillium citrinum*,[18,19] and proteases.[20–23] The Mannich reaction is one of the most useful synthetic strategies for the preparation of β-amino carbonyl compounds through C-C bond formation reactions.[24] Acquiring precise knowledge about mechanistic aspects of enzyme catalytic promiscuity paves the way for directed evolution and designing enzymes with increased catalytic activity and rationally controlled substrate specificity and stereoselectivity.[25,26] Up to this time, only a few reports have been published on reactions catalyzed by hen egg white lysozyme (HEWL) (EC 3.2.1.17), and mechanistic studies of these promiscuous reactions have not been scrutinized deeply. The first HEWL-catalyzed promiscuous reaction was aza-Diels-Alder three-component reaction, and it was proposed a related mechanism based on suggested active sites (D52 and E35) by crystallographic studies.[27,30] Second and third reports were related to the promiscuous C-C coupling reaction for the synthesis of conjugated polyacetylene and 3-indolyl-3-hydroxy oxindole.[31,32] Previously reported enzymatic Mannich reactions include lipase from *Mucor miehei* (MML)[33] and lipase B from *Candida antarctica* (CAL-B).[34] Furthermore, both acylase from *Aspergillus melleus* and protease type XIV from *Streptomyces griseus* (SGP) were employed in acetonitrile medium for 96 h to carry out the asymmetric Mannich reaction[22,35]; in all the cases, the reaction time was much longer and the aldol reaction occurred as a side reaction. Additionally, enzymes have a series of problems including difficult recovery, thermal instability, and loss of activity in adverse conditions when used as biocatalysts. An effective method to address the above defects would be enzyme immobilization. The immobilizing can help the reactivity, stability, and recyclability of the enzyme by maintaining the catalytic properties of the enzyme, improving catalytic properties under a variety of reaction circumstances through attracting substrates near the active site and enhancing reaction kinetics.[36,37] A novel class of nanomaterials called metal-organic frameworks (MOFs), which are made of organic ligands and metal-containing nodes, have been developed for a broad range of applications such as gas storage, separation, drug delivery, and immobilization of enzymes and other biomolecules.[38] Following enzyme encapsulation, MOFs have gained enormous attention for high surface area, superior chemical, structural stability, and maintaining catalytic activity than alternative immobilization techniques due to their

[1]Biochemistry and Chemical Biology Research Laboratory, Department of Chemistry, Sharif University of Technology, Tehran, Iran
[2]Lead contact
*Correspondence: kalhor@sharif.edu
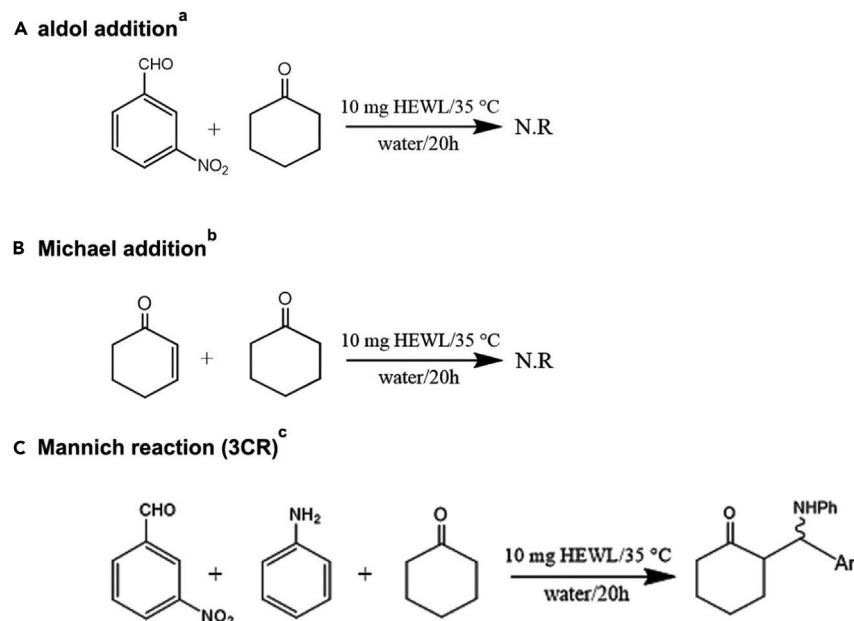
Scheme 1. Using HEWL as biocatalyst in C-C coupling reaction

Aldol, Michael, and Mannich reactions catalyzed by HEWL, reaction conditions:

(A) A solution of 3-nitrobenzaldehyde (0.2 mmol), cyclohexanone (0.1 mmol), HEWL (10 mg), and water (1 mL) was stirred at 35°C for 20 h.

(B) A solution of cyclohexanone (0.1 mmol), 2-cyclohexenone (0.1 mmol), HEWL (10 mg), and water (1 mL) was stirred at 35°C for 20 h.

(C) A solution of 3-nitrobenzaldehyde (0.1 mmol), aniline (0.11 mmol), cyclohexanone (0.17 mmol) HEWL (10 mg), and water (1 mL) was stirred at 35°C for 20 h.
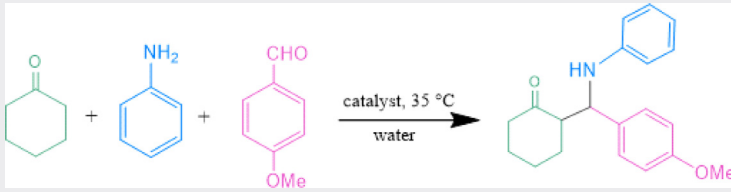
regular crystal structure and high stability; in addition, it has been demonstrated that MOFs can have a protective effect for encapsulated enzymes in adverse circumstances leading to aggregation and unfolding.[39–41] In general, there are two types of techniques for immobilizing enzymes: (1) *De novo* encapsulation (DNE), *in situ* encapsulation within the framework, and (2) Post-synthetic encapsulation (PSE), immobilization on the surface or diffusion into the pores; recently, it was demonstrated that the embedding efficiency of *in-situ* enzyme encapsulation in MOF could be enhanced in the presence of peptide as a co-ligand, and the stability and recovery activity of the enzyme were also increased,[42] In another report, the post-synthetic encapsulation was used to immobilize catalase on the surface of amino-functionalized MIL-125-NH₂ to enhance activity recovery, pH stability, and thermostability of the enzyme.[43] A subclass of MOFs known as zeolitic imidazolate frameworks (ZIFs) typically consists of huge cavities connected by small windows.[44] In recent years, enzymes encapsulated in ZIFs have been used in biological applications such as synergistic tumor therapy and chemotherapy.[45] In addition, ZIFs are desirable templates for enhancing enzyme's activity and stability, carrying out enantioselective enzymatic reactions,[46] constructing biosensors,[47] and cascade reactions.[48] Due to their biocompatibility,[49] gentle synthesis reaction conditions, structural variety, enormous specific surface area, high porosity, and great water stability, ZIFs have been under the spotlight.[50–53] The ZIF was also observed for encapsulation of glucose oxidase into microporous zeolitic imidazolate framework-8 with 3-mercaptophenylboronic acid, in order to improve affinity and catalytic efficiency compared to free glucose oxidase.[54]

In the present work, we have investigated the catalytic application of HEWL in the formation of Mannich adducts via the one-pot three-component reaction in aqueous media in 9–16 h; moreover, the efficiency of the encapsulated enzyme in a metal-organic framework and its recyclability for Mannich reaction were investigated. Additionally, we have looked deeper into the mechanism of catalytic promiscuity using site-directed mutagenesis, molecular docking, and molecular dynamic simulations to clarify the role of the catalytic active site residues.

RESULTS AND DISCUSSION

Biotransformation of C-C bond by hydrolases

In order to assess organic biotransformation using hydrolases two hydrolytic enzymes named protein splicing (intein) and hen egg white lysozyme were examined. A number of canonical C-C formation reactions: aldol condensation, Michael, and Mannich reactions were investigated. As shown in Scheme 1, to our surprise only Mannich reaction was catalyzed by HEWL (EC 3.2.1.17) in high yields. In the three-component Mannich reaction, an amine (aniline), an aromatic aldehyde (benzaldehyde), and an unmodified ketone (acetone and in some cases cyclohexanone) were directly (three substrates simply were added to one vessel simultaneously) and indirectly (the aldehyde and amine were mixed to form the Schiff base first) used. The reaction products were confirmed using ¹H NMR and ¹³C NMR (see method details and Figures S1–S23). To investigate the optimal amount of the enzyme in the Mannich reaction, different amounts of HEWL (1, 5, 10, and 20 mg of enzyme) were used. It turned out that 20 mg of the enzyme was the optimal amount in the shortest reaction time. To gain further insight into the catalytical

Table 1. Control experiments for the HEWL-catalyzed three-component Mannich reaction

Entry[a]	Catalyst	Yield (%)[c]
1[b]	Hen egg white lysozyme (HEWL)	70
2	BSA	trace
3	Mycobacterium tuberculosis RecA (Mtu-H37Rv RecA)	28
4[d]	Denatured HEWL	35
5[e]	urea	35
6[f]	No enzyme	23

[a]Unless otherwise noted, the reaction conditions were as the followings: Cyclohexanone (0.5 mmol), 4-methoxybenzaldehyde (0.3 mmol), and aniline (0.33 mmol) were added to a solution of catalyst (20 mg) in deionized water (1mL), and the reaction mixture was stirred at 35°C.
[b]The reaction carried out for 16 h.
[c]The yield was determined by analysis of crude products.
[d]HEWL was pre-treated with urea (6 M) at 60°C for 20 h.
[e]Urea (1mL, 6 M) was used instead of HEWL.
[f]The reaction was carried out for 72 h.

activity of the biocatalyst, a variety of control experiments were performed using cyclohexanone, 4-methoxybenzaldehyde, and aniline as the substrates in the reaction (Table 1). In the absence of the enzyme, the Mannich adduct was only obtained in 23% yield after 72 h, indicating that HEWL had a catalytic activity for the reaction (Table 1, entry 6). When BSA, a non-enzyme protein, and an intein, a self-splicing protein, were used, Mannich products were obtained in trace and 28% yield, respectively (Table 1, entries 2 and 3). These results demonstrated that the Mannich reaction required some active residues that were present in the structure of HEWL. To answer the question of whether a folded structure of the enzyme was involved in catalyzing the reaction or not, urea and urea-denatured HEWL were used in the model reaction; both conditions gave 35% yield for the Mannich adduct (Table 1, entries 4 and 5), indicating a folded structure of the enzyme was needed for catalyzing the promiscuous Mannich reaction.

Scope of biotransformation by HEWL

To further look into the scope of the biotransformation, a number of derivatives for benzaldehyde, aromatic, and aliphatic amines were examined by the action of HEWL (Table 2, entries 1–9). More importantly, the data supports that HEWL was able to bind a wide range of aldehyde derivatives for making β-amino carbonyl compounds. Furthermore, aromatic amines containing electron-withdrawing groups and aliphatic amines were also examined in the reaction, and the results showed moderate to high yields. Generally, aliphatic amines are more nucleophilic than aromatic amines; especially the presence of electron-withdrawing substituents on aromatic rings would increase this difference. Indeed, a higher yield for aliphatic amine was expected; however, the data shown in Table 2 (entries 8 and 9) indicate the opposite. This observation can be explained due to protein-substrate π-stacking interactions which are more favorable. Similar results were detected in the presence of cyclohexanone (Table 3).
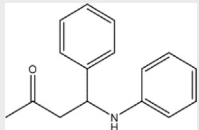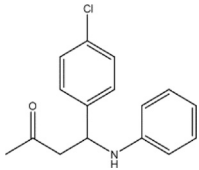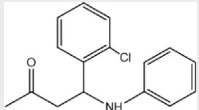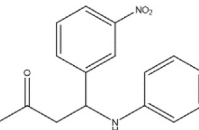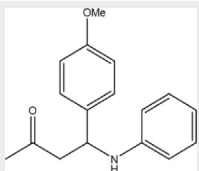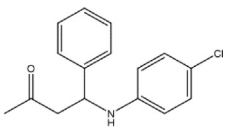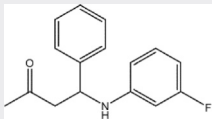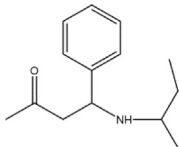
Diastereo-, enantio-, and chemoselectivity by HEWL

In order to delineate whether the products of the reaction are syn or anti, cyclohexanone was used in place of acetone in a three-component Mannich reaction (Table 3). The presence of electron-withdrawing or electron-donating groups on aldehyde and arylamines had no significant impact on diastereoselectivity, indicating thermodynamic control of the diastereoselective Mannich reaction. To further investigate the enantioselectivity of the HEWL-catalyzed Mannich reaction, some selected Mannich adducts with varying substituents were examined. The HPLC results demonstrated that the HEWL-catalyzed Mannich reaction produced only racemic mixtures (see Table S1 and Figures S24–S29).

Recyclability of HEWL and structural studies
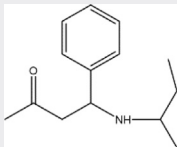
To illuminate whether the chemical environment of reactions and the recycling of the enzyme for multiple times could have adverse structural consequences for the enzyme, intrinsic fluorescence and CD spectroscopy were measured. As shown in Figure S30A, the wild-type enzyme (in the absence of any chemical substance) displayed characteristic absorbance peaks at 208 nm and 222 nm for α-helices, in addition to the

Table 2. Investigation of the substrate scope for HEWL and mutated HEWL-catalyzed Mannich reaction with acetone

$$R^1CHO \;+\; R^2NH_2 \;+\; \text{(acetone)} \xrightarrow[\text{water/9h}]{\text{HEWL(20mg)/35 °C}} \text{product}$$

Entry[a]	R¹	R²	Product	Time (h)	Yield (%)[b]	Yield (%)[c]
1	Ph	Ph		9	78	88
2	4-ClC₆H₄	Ph		9	80	89
3	2-ClC₆H₄	Ph		9	82	ND
4	3-NO₂C₆H₄	Ph		9	78	ND
5	4-OMeC₆H₄	Ph		9	72	85
6	Ph	4-ClC₆H₄		9	73	85
7	Ph	3-FC₆H₄		9	72	ND
8	Ph	*Sec*-butyl		9	52	60

(Continued on next page)

Table 2. Continued

9	Ph	Me		9	50	ND

[a]Reaction conditions: a solution of aldehyde (0.3 mmol), amine (0.33 mmol), acetone (0.5 mmol), HEWL (20 mg) in deionized water (1 mL) was stirred at 35°C for 9 h.
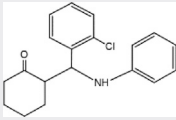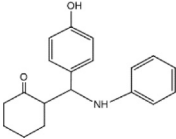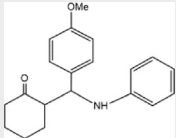[b]Yields of isolated products.
[c]Mutated HEWL (D52A) was used as biocatalyst; ND: not determined.

peaks at 215–218 nm for β-sheets (The secondary structure contents of native HEWL during three successive recycling is provided in Table S2). When the enzyme carried out the reaction and subsequently was recovered as explained in method details, its CD absorbance displayed remarkably similar peaks as the wild-type enzyme. This observation itself demonstrated that the chemical environment of the reaction and manipulation of the enzyme did not change the secondary structure of the protein. As HEWL was recycled from the reaction for the fourth time, the secondary structure of the protein was significantly altered. The alteration was mainly due to the loss of anti-parallel β-sheet, but no conversion to the β-sheet structure was observed; however, based on previous studies, conformational change to β-sheet structure had been reported as the hallmark of amyloid and aggregation,[55] indicating that the enzyme was not aggregated during the recycling. Interestingly, the activity of the recycled enzyme followed exactly the structural changes by CD, explaining the reduction of activity due to the structural modification. To further look into the overall 3D structure of the enzyme, intrinsic fluorescence was obtained after multiple recycling of the enzyme (see Figure S30B). Tryptophan intrinsic fluorescence usually decreases as the protein undergoes an unfolding process since the Trp residues would be exposed to solvent (water). In the case of HEWL enzyme, the opposite observation was taking place due to polar residues (e.g., Cys and Ser) near a tryptophan in the fully folded state.[56] As HEWL unfolds the Trp residues would be going away from the polar residues, and therefore the intrinsic fluorescence would be increased. As shown in Figure S30B, as the recycling number increased, the Trp fluorescence also amplified, indicating the similar phenomena with the CD absorbance. To further investigate the effect of reusability on the

Table 3. Investigation of the substrate scope for HEWL-catalyzed Mannich reaction with cyclohexanone

Entry[a]	R[1]	R[2]	Product	Time (h)	Yield (%)[b]
1	2-ClC$_6$H$_4$	Ph		9	78
2	4-OHC$_6$H$_4$	Ph		16	70
3	4-OMeC$_6$H$_4$	Ph		16	70

[a]Reaction conditions: a solution of aldehyde (0.3 mmol), amine (0.33 mmol), cyclohexanone (0.5 mmol), and 20 mg HEWL in deionized water (1 mL) was stirred at 35°C for 16 h.
[b]Yields of isolated products.
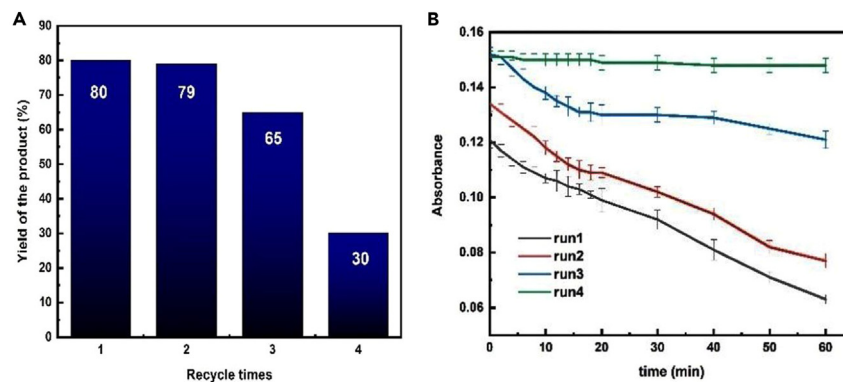
Figure 1. Biological activity of recovered HEWL

(A) Catalytic performance of the reused HEWL after 4 runs on the yield of 4-(3-nitrophenyl)-4-(phenylamino)butan-2-one. Reaction conditions: a solution of 3-nitrobenzaldehyde (0.3 mmol), aniline (0.33 mmol), acetone (0.5 mmol), water (1 mL) HEWL 20 mg, reaction temperature of 35°C and reaction time 9 h.

(B) Turbidimetric assay of recycled HEWL: 0.25 mg/mL of *Micrococcus luteus* (*M. luteus*) cell suspension was incubated with 1 mg/mL of each recycled lysozyme run. The decrease of turbidity at 450 nm confirmed that the muramidase activity of lysozyme would dramatically decrease after reusing the enzyme 4 times, error bars indicate standard deviation.

product yield, the Mannich reaction of 3-nitrobenzaldehyde, aniline, and acetone in the presence of recycled HEWL of each step was carried out. The results showed that the most enzymatic activity had been lost during the recycling (Figure 1A).

Biological activity of recovered HEWL

To further assess the biological activity of HEWL through multiple cycling reactions, the turbidimetric assay was performed. The turbidimetric assay demonstrated that as the enzyme went through more cycles of reactions its muramidase activity failed dramatically, especially in run 4 (Figure 1B). Considering the enzymatic activity of HEWL after recycling, and the similar trend that was observed for both enzymatic activities of HEWL and the yield of Mannich product, it can be suggested that the same active site that would be responsible for muramidase activity may also be involved in the Mannich reaction.

Immobilization of HEWL and characterization

As reported previously, the recovery and reusability of HEWL were difficult and inefficient. In addition, HEWL, after three cycles of reaction, had lost part of its tertiary structure; therefore, encapsulation may aid in folding and recycling the enzyme. To encapsulate HEWL, ZIF-8 was selected as an encapsulator. HEWL's structural dimension (ellipsoid radii in pH = 7: a = 2.40, b = 1.31, and c = 1.12 nm) is smaller than ZIF-8's cavity (600 nm),[57,58] and presumably the pore apertures and diameters of ZIF-8 are smaller than the enzyme, allowing for successful HEWL encapsulation without HEWL leaking.[59] As previously reported, low-Zn^{2+}/2-methylimidazole (2-mIM) ratio (1:4 and 1:8 metal/ligand ratio) would lead to generate active biocomposites with predominantly sod topology[60]; thus, HEWL/ZIF-8 biocomposites were synthesized using 1:4 Zn^{2+}/2-mIM concentration under different conditions to improve immobilization.[61]

Because of the positive surface charge of HEWL, the yield for the synthesis of biocomposite turned out low. To solve this problem, poly-vinylpyrrolidone (PVP) was used as an assistant for the dispersion and stabilization of the enzyme in water. The PVP-modified HEWL-His/ZIF-8 (abbreviated as PHHZ biocomposite) was produced as explained in method details. To confirm that the HEWL-His/ZIF-8 has been synthesized and that the surface adsorption of the enzyme had been removed, the Fourier transform infrared spectroscopy (FT-IR), X-ray diffraction analysis (XRD), scanning electron microscopy (SEM) and some other analyzes were performed. As shown in Figure 2, the FT-IR spectra indicated that in the presence of polyvinylpyrrolidone (PVP) as an enzyme stabilizer and encapsulation promoter, the enzyme immobilization was formed much better than the other immobilization conditions. The FT-IR fingerprint region confirmed the typical ZIF-8 modes, including the peak at about 420 cm^{-1} related to the Zn–N stretching mode and the peaks at about 692, 750, 953, and 1306 cm^{-1} due to out-of-plane bending and in-plane bending of imidazole aromatic ring, respectively. An absorption peak at about 1600–1712 cm^{-1}, which corresponded to the C=O stretching in the carboxyl group, belonged to the amide I bond, signifying the presence of HEWL in the biocomposite.[62,63] Although histidine characteristic peaks, in the yellow color spectrum, are not well defined in the HEWL-His/ZIF-8 spectra, the peaks indicate that the encapsulation efficiency of the enzyme in the presence of L-His is improved. In order to examine whether the enzyme is adsorbed on the surface or immobilized inside the ZIF-8, the surface adsorption of the enzyme on the structure of ZIF-8 in the presence and the absence of PVP was analyzed using FTIR (Figure 2) and SEM (see Figure S31). The results indicated that the structure of ZIF-8 was completely different from PHHZ, confirming the immobilization of the enzyme inside the ZIF-8.

The XRD pattern of the pure ZIF-8 and PHHZ is displayed in Figure S32. The diffraction peaks at 2θ = 7.4°, 10.4°, 12.8°, 14.7°, 16.5°, 18.1°, 22.1°, 24.5°, 25.7°, and 26.7° for the resulting pure ZIF-8 were compared with previously published data of ZIF-8 crystal in literature. It is clear that the XRD pattern of PHHZ agrees well with those of ZIF-8. These results also confirm that the immobilization of the enzyme did not affect the crystallinity of ZIF-8, and that the successful synthesis of the PHHZ has been realized.[64]
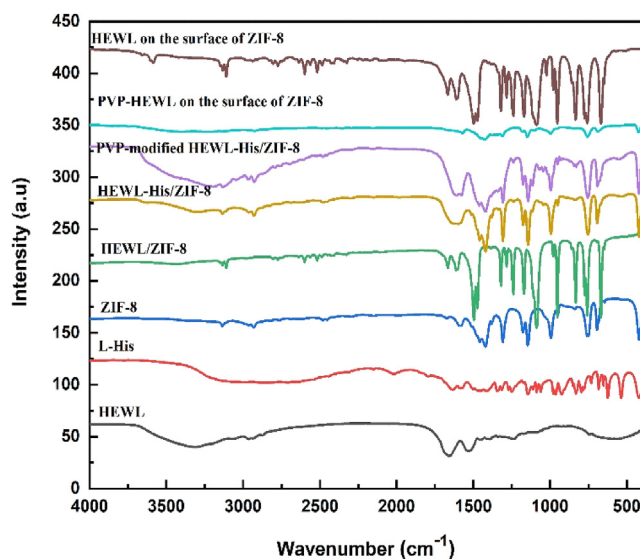
Figure 2. FT-IR spectra of different HEWL-biocomposites

FT-IR spectra of pure HEWL, L-His, ZIF-8 crystal, HEWL/ZIF-8, HEWL-His/ZIF-8, PVP-modified HEWL-His/ZIF-8, and adsorbed HEWL on the surface of pre synthesized-ZIF-8 in the presence and absence of PVP.

SEM images were recorded to investigate the morphology of the biocomposites, the size of the prepared PHHZ, and the growth process. As shown in Figure 3B, HEWL-His/ZIF-8 without further PVP modification, showed ZIF-8-like SOD topology with a particle size of 500 nm-1.5 μm and some agglomeration which was probably due to the surface enzyme adsorption. Meanwhile, the PHHZ demonstrated a better SOD topology with slightly larger dimensions and without agglomeration (Figure 3C). The XRD and SEM results showed that the encapsulation of the enzyme inside the ZIF-8 did not change the crystal structure markedly, but it led to an increase in the particle size of the final biocomposite. Additionally, to further confirm the presence and distribution of HEWL in the biocomposite, the energy-dispersive X-ray spectroscopy (EDX) mapping of ZIF-8, HEWL-His/ZIF-8, PHHZ, and adsorbed HEWL on ZIF-8 were performed. As shown in Figures S33–S38, the percentage of sulfur, which indicates the presence of enzyme in the structure, is increased in the PHHZ. Additionally, the elemental mapping images demonstrate a good distribution of sulfur, which most likely indicates the low possibility of accumulation of enzyme in the structure.

To further examine the immobilization of enzyme in the ZIF-8 structure, thermogravimetric analysis (TGA) was performed (see Figure S39); it was demonstrated that in the range of 200–600°C, the mass of PHHZ was significantly reduced while the mass of ZIF-8 almost stayed the same, emphasizing the presence of HEWL in the structure of ZIF-8. Based on the TGA analysis, the temperature at 320°C was selected for calcination for 2 h to remove HEWL molecules from the biocomposite without destroying the ZIF-8 structure.[65] The SEM images of PHHZ before and after calcination revealed some small cavities, corresponding to the partial thermal degradation and removal of enzyme (comparing Figures S31A and S31B), showing that the enzyme was immobilized inside the ZIF-8 structure. When the surface adsorbed enzyme on the ZIF-8 was calcined, SEM and FT-IR results showed that surface adsorption generally changed the structure of ZIF-8, confirming that the structure was not adsorbed on the surface, and after calcination, the structure was completely destroyed (see Figures S31C and S31D).

### Efficiency, maximum loading, and activity of immobilized enzyme

As explained in method details, the immobilization efficiency was measured for PHHZ as 73.6% and for the surface adsorbed HEWL as 52%. The maximum loading was also calculated for the encapsulated enzyme with different amounts of enzyme after 24 h; as shown in Figure S40, after the washing step, the maximum loading of the enzyme immobilized ZIF-8 had reached 0.3 mg of enzyme/mg of ZIF-8.[66]

To observe the effect of immobilization on HEWL activity, the lytic activity against *M. luteus* was measured using UV-Vis spectrophotometer as described in method details.[67] As shown in Figure 4, it was realized that the activity of the immobilized enzyme for the native reaction was very similar to the free enzyme. The little difference in the activity between free and immobilized enzymes was most likely due to the difficulty of the immobilized enzyme to access sufficient amounts of bacterial cells. As previously reported,[42,43] the activity recovery of immobilized HEWL is defined as the ratio of total activity of immobilized HEWL to the total free HEWL activity; therefore, the activity value of 89.5% is calculated for the immobilized enzyme, this result indicates that the activity of free enzyme in turbidity assay is higher than the immobilized enzyme.

Furthermore, kinetic parameters of the enzyme were obtained by determining the initial reaction rates with *M. luteus*, as explained in method details. As shown in Table S3 and Figure S41, the K_m value for immobilized-HEWL was higher and the V_{max} value was lower than free-HEWL, it is possible that the ZIF-8 has mass transfer resistance for *M. luteus*.[68]

Furthermore, the encapsulated enzyme was investigated as a biocatalyst for Mannich reactions with electron-donating and -withdrawing functional groups and aliphatic amine under the same reaction conditions (Table 4), emphasizing that the amount of enzyme immobilized in
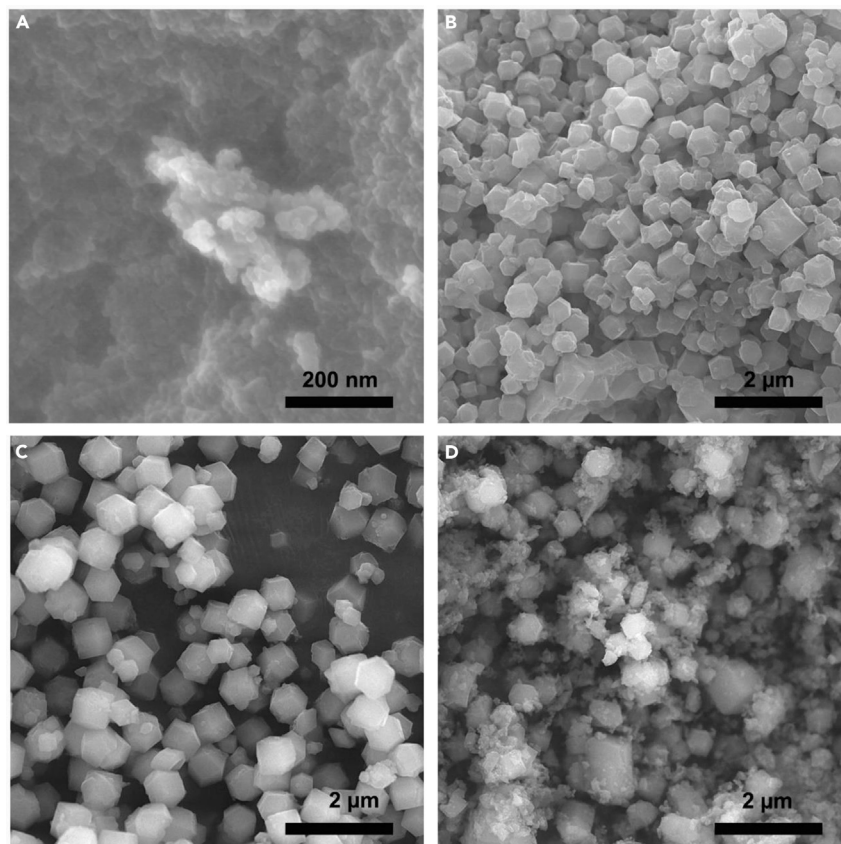
Figure 3. SEM images of composites
(A) ZIF-8.
(B–D) HEWL/ZIF-8 in the presence of L-His (B) without, and (C) with PVP modification, and (D) reused catalyst after 7 cycles.
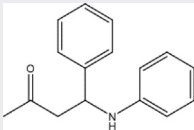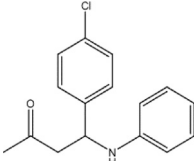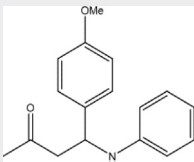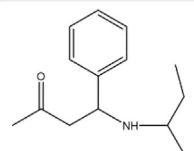
ZIF-8 was calculated as 5.5 mg. In almost all cases, the yield of the product was increased, most likely, because of bringing more substrates near the active site of the enzyme and enhancing the reaction kinetics, leading to a faster reaction rate. It must be noted that ZIF-8 was unable to carry out the reaction on its own. The superior folding of the enzyme in ZIF-8, the maintenance of the 3D structure throughout the reaction,
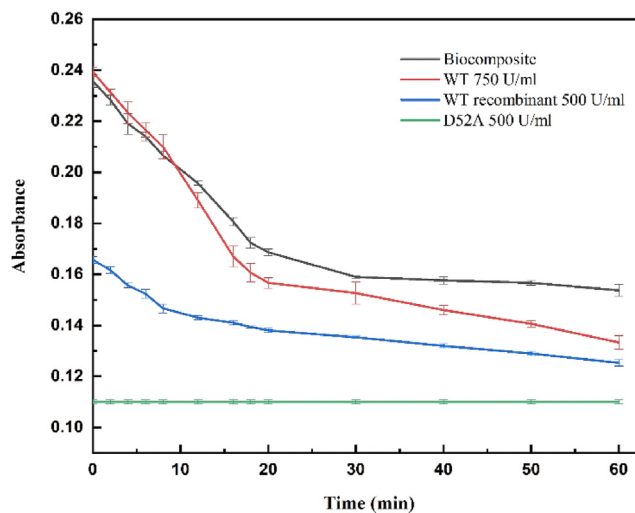
Figure 4. Turbidimetric assay of wild-type lysozyme, PHHZ, and mutant D52A against *M. luteus*
The absorbance was measured as described in the legend of Figure 1B for the recycled HEWL; error bars indicate standard deviation.

Table 4. Investigation of the substrate scope for Mannich reaction catalyzed by PHHZ

Entry[a]	R[1]	R[2]	Product	Time (h)	Yield (%)[b]
1	Ph	Ph		9	85
2	4-ClC$_6$H$_4$	Ph		9	85
3	4-OMeC$_6$H$_4$	Ph		9	83
4	Ph	*Sec*-butyl		9	60

[a]Reaction conditions: a solution of aldehyde (0.3 mmol), amine (0.33 mmol), acetone (0.5 mmol), PVP-modified HEWL-His/ZIF-8 (20 mg) in deionized water (1 mL) was stirred at 35°C for 9 h.
[b]Yields of isolated products.

and the increased accumulation of the substrate near the enzyme appeared to offset the decrease in the amount of enzyme in the reaction when employing PHHZ instead of free HEWL.

After confirming the catalytic activity of the PHHZ in performing the Mannich reaction, analytical chiral HPLC was used to determine the enantioselectivity of the Mannich reaction product (in the presence of the PHHZ) and estimate the percentage of racemization occurring during the synthesis. The results showed that the synthesis of the Mannich reaction product in the presence of the PHHZ, was the same as the free enzyme, generating almost racemic products and there was little variation in the proportion of R and S products (the screening results are reported in the supplemental information, Figure S29).

Reusability of PVP-modified HEWL-His/ZIF-8

The PHHZ bio-composite activity was measured 7 cycles (Figure 5). After the completion of each reaction, the encapsulated enzyme was then recycled by a simple centrifugation and again the same amount of weight was used in the next reaction. The reusability of HEWL was significantly improved and was enhanced upon encapsulation in the ZIF-8. Additionally, the ZIF-8 was able to play a protective role in the enzyme activity. PHHZ activity was retained after 6 cycles but in the 7th cycle, the yield decreased dramatically. Figure 3D demonstrates the morphology of the PHHZ after 7 recovery cycles, indicating that the structure of PHHZ was deformed.

Characterization of hen egg white lysozyme variant (Asp52Ala)

To further look into the mechanism of the HEWL-synthesized beta-amino carbonyl products, site-directed mutagenesis was implemented. Asp52Ala variant of HEWL lacking the basic catalytic residue in the active site was generated (see Figures S44–S47 and Table S6). The bactericidal activity of wild-type (recombinant) lysozyme and D52A mutant against gram-positive bacteria (*M. luteus*) was measured. From the results of Figure 4, it was deduced that mutant lysozyme was enzymatically inactive toward its natural substrate as the mutant lacked the nucleophilic residue of the active site to create the covalent intermediate.

The ability of wild type and D52A mutant of HEWL to catalyze the Mannich reaction was examined in aqueous media. Interestingly, the enzymatically inactive Asp52Ala mutant displayed an increased reaction rate when the Mannich reaction was catalyzed as compared to the wild-type lysozyme (Table 2). In a previously published report, using HEWL to perform Aza-diel-alder reactions, it was suggested that
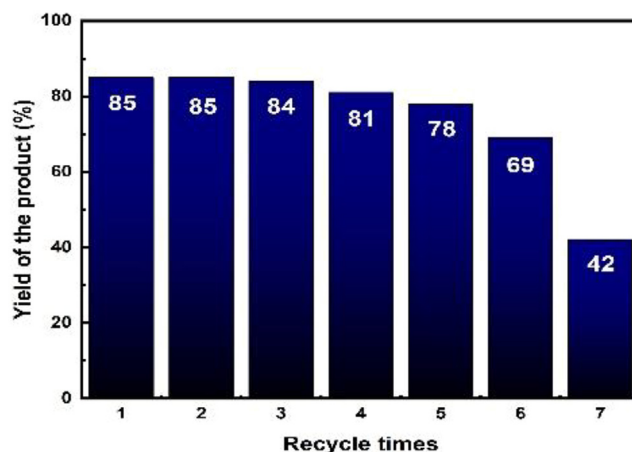
Figure 5. Catalytic recyclability of PHHZ for the Mannich reaction
The PHHZ biocomposite was used for a solution of benzaldehyde, aniline, and acetone as substrates in the model reaction.

under acidic conditions provided by Glu35, an equilibrium between enol form and keto would occur, consequently, Asp52 could act as a nucleophile and abstract the acidic proton.[27] Although our site-directed mutagenesis result indicated that Asp52 interrupted the natural hydrolase activity toward the peptidoglycan cell wall, it had no catalytic role in the promiscuous mechanism of the non-natural substrate and additionally increased Mannich's reaction rate. Based on crystallographic studies reported in 1996,[69] the mutant lysozyme has the same structure as the wild-type lysozyme, indicating that the increase in catalytic efficiency is not due to structural changes caused by the mutation and new interactions induced by the mutation may be responsible for the higher reactivity.

Computational studies of lysozyme's promiscuous reaction

In order to elucidate the observed reactivity differences between the wild-type and D52A mutant enzyme, computational studies into the binding of the substrates in the HEWL active site were performed, showing that reactivity differences could truly arise from the stage of substrate binding. These results revealed a different strategy for the promiscuous reaction catalyzed by HEWL. As illustrated in Figure S42, aniline, benzaldehyde and acetone as model ligands were docked into the entire surface of HEWL crystallographic structure (PDB: 2EPE), to investigate the ligand-protein interactions (for details, see Table S4). As reflected in Figure S42, there exist non-covalent interactions such as hydrophobic and π-stacking interactions through aliphatic residues (Ile98, Ala107, and Asn59) and an aromatic residue (Trp108, Trp63) for aniline and benzaldehyde; moreover, the presence of hydrogen bonding via main-chain of Gln57 and Asn59 are evident. It may be suggested that following the formation of protonated Schiff base (highly active), in the binding pocket of the enzyme, acetone as an unmodified ketone by hydrophobic and H-bond interactions undergoes keto-enol tautomerism to stabilize the enolate anion and proceed the Mannich reaction.

To gain more details on the binding of the enzyme to the non-native substrates, molecular dynamics (MD) simulations were performed. To analyze the enzyme-substrate complex and its behavior throughout the simulations, RMSD and gyration were calculated for 10 ns (see Figure S43). The important interactions of HEWL with the substrate and the intermediate were examined sometimes at the end of the simulations (Figure 6). The MD snapshot corroborated what docking demonstrated for wild-type HEWL in Figure S42, the H-bond and π-stacking interactions of the substrate through residues lead to the correct placement of starting materials in relation to each other and the formation of imine (Figures 6A and 6B). Notably as can be seen in Figures 6C and 6D, it is important to mention that the presence of water has a crucial role in the formation of an enolate anion, because of the abstraction of acidic hydrogen by water molecules. Interestingly, the orientation of acetone in the mutated enzyme is somewhat different from the wild type (Figure 6D); that is, acetone as a substrate located on the less crowded side near the Schiff base. This positioning, the presence of Arg112, and some water molecules near acetone (especially the water molecule that has a hydrogen bond with the Schiff base and Trp62) might better explain the activity of the mutant as compared to the wild type.

Based on the mutagenesis experiment, molecular docking, and molecular dynamics analyses, a plausible mechanism for the Mannich reaction performed by HEWL is proposed in Scheme 2. Although numerous studies on the structural and enzymatic characteristics of hen egg white lysozyme have been reported, its mechanism of catalytic promiscuity has not yet been fully understood. Since the acidity of amino acids in the active site of the enzyme is moderately low, protonation of nitrogen is more probable than the protonation of oxygen on aldehyde giving rise to a no aldol side reaction (Scheme 1). On the basis of crystallographic evidence for native HEWL[70] in addition to biochemical and crystallographic studies on Asn59 mutant,[71] a hydrogen-bonding platform between enzyme residues (Asp52, Asn46, Asn59, Ser50, and Asp48) on the anti-parallel β-sheet exists. Studies have demonstrated that Asn59 plays a critical role in the hydrolytic activity, hydrolysis of the bacterial cell wall, and protein-carbohydrate interaction of HEWL. Indeed, in the mutant Asp52 where the direct interaction between Asp52 and Asn59 side chains no longer exists, the orientation of Asn59 is affected to provide a binding site for the substrate as a new hydrogen bonding network.
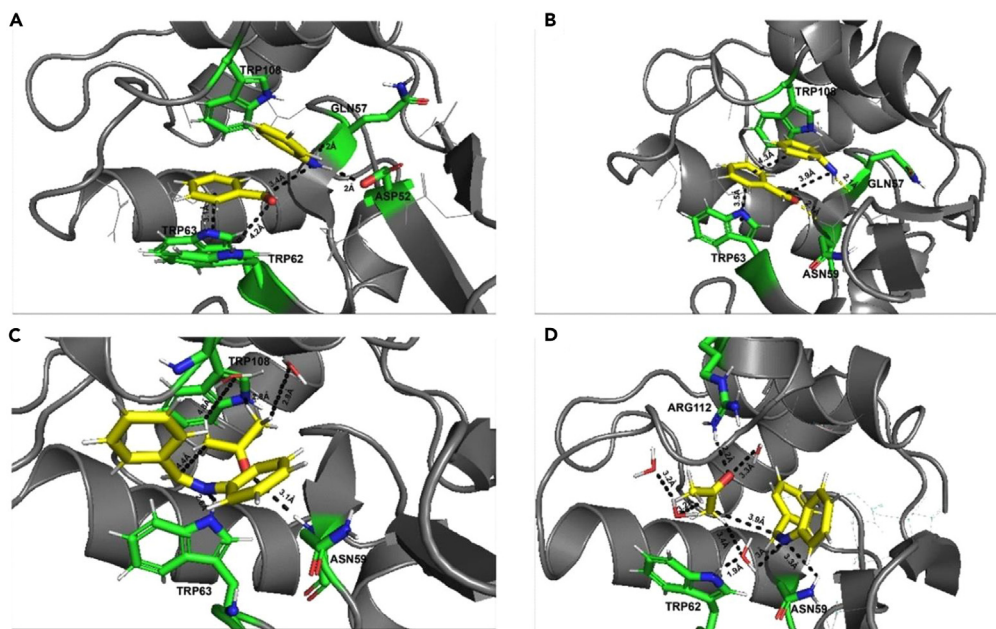
Figure 6. Snapshots of randomly positioned of simulations for HEWL complex with substrates and the intermediate
(A and B) Interactions of aniline and benzaldehyde with wild-type HEWL and mutated HEWL.
(C and D) Schiff base and acetone interactions with wild-type HEWL and mutated HEWL respectively. Hydrogen bonds are depicted as dotted lines. The water molecules are displayed as white and red molecules. All images were generated using PyMOL.

The proposed mechanism for wild-type HEWL catalyzed reaction, based on our results is as follows; first, Trp62 could stabilize the partial negative charge on the carbonyl functional group of aldehydes via hydrogen bonding. Gln57 located in β-sheet accommodates aniline through hydrogen bonding from the main-chain oxygen atom. In the neutral solution, the reaction between primary amine and aldehyde produces the carbinolamines, however, the formation of a Schiff base requires an acidic or basic condition.[72] Given that, Trp62 assisted by Gln57 may accelerate the formation of the hemiaminal and prepare a proper environment for subsequent Schiff base protonation (excellent electrophile). Protonation of the Schiff base is preceded by hydrogen bonding employing Trp63. The most important step in the formation of β-aminoketones is keto-enol tautomerization. Second, the backbone amide of Asn59 could act as an oxyanion hole and stabilize the negative charge formed on oxygen in the enolate. At the same time, the presence of one water molecule seems to be essential to move forward the reaction and abstract the hydrogen from ketone. Last, a new carbon-carbon bond is formed and Mannich adduct is released from the oxyanion hole. The proposed mechanism is also supported by the results obtained from intrinsic tryptophan fluorescence of recycled HEWL, which suggested that as the enzyme unfolds and Trp residues move away from the sulfur atom (e.g., Met or Cys) the yields of the Mannich reaction gradually decrease (see Figure S30B). In the mutated enzyme, π-stacking interactions (benzaldehyde-aniline and benzaldehyde-Trp63) and hydrogen bonds (between benzaldehyde-Asn59 and aniline-Glu57) play an important role in the stability of the substrates in the active site. Unlike wild-type HEWL, in the mutated version, Arg112, positioned near acetone, could act as an oxyanion hole by forming a hydrogen bond and facilitating the formation of enolates. The water molecule, present in the active site of the mutated HEWL, between acetone and Schiff base, could easily abstract the α hydrogen from ketone and exchange hydrogen with aniline (Figure 6D).

Although a few numbers of biocatalysts have been identified to perform Mannich reactions, as mentioned in the introduction, none of the studies has been able to use aliphatic amine as a reaction substrate. As shown in Table S5, the reaction times with other biocatalysts were very long; the use of organic solvents in most cases, using a large amount of ketone to perform the reaction, and the inability of the enzyme recovery are other limitations of the previous works.

Limitations of the study

One of the shortcomings in using HEWL in Mannich reaction might be its lack of stereoselectivity. However, investigating the role of MOF in stereoselectivity of HEWL in performing the promiscuous reaction could be imperative. Another shortcoming relates to the difficulty of immobilization of recombinant enzymes, in general, inside of ZIF-8. It would be intriguing to examine the immobilization of the mutated enzyme D52A in performing Mannich reaction.

Conclusions

In the present work, a new mechanistic aspect of the HEWL-catalyzed one-pot three-component Mannich reaction was demonstrated. Not only does performing Mannich reaction by HEWL benefits from being in aqueous media and under mild reaction conditions but also lysozyme
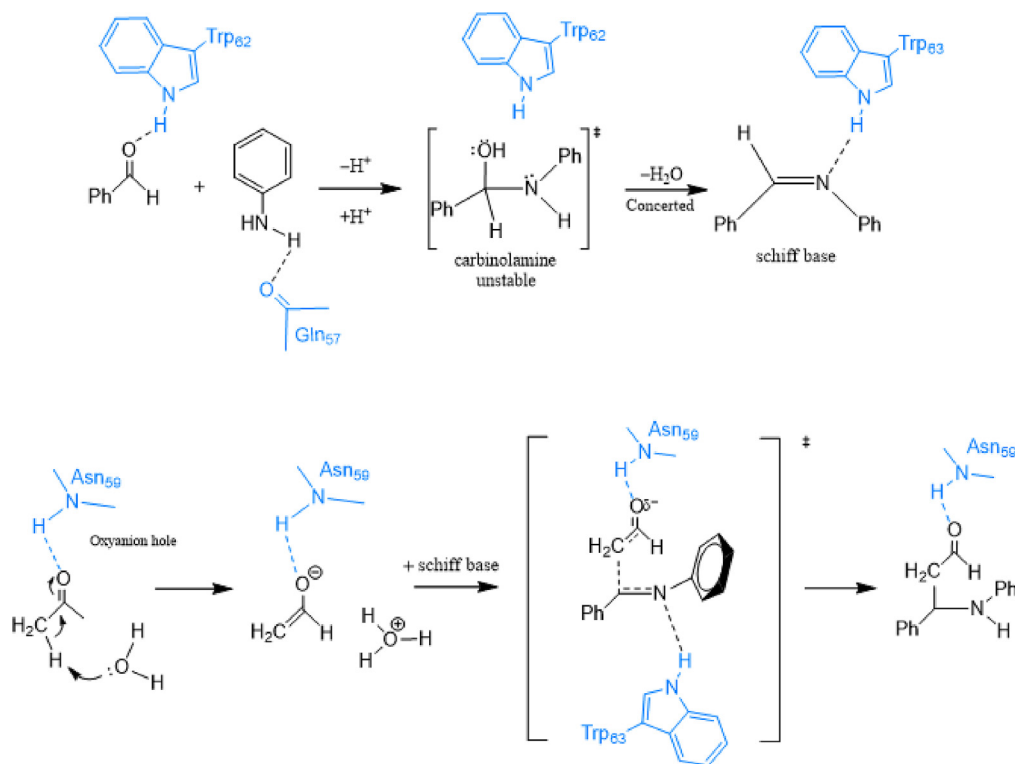
Scheme 2. Proposed mechanism of HEWL-catalyzed Mannich reaction based on molecular docking and molecular dynamic studies.

encapsulated in ZIF-8 improved the yield of the products and recyclability of the enzyme. Simple work-up, a wide range of substrates including aliphatic amine, and exploiting unmodified ketones are other advantages of the reported strategy as well. Moreover, replacing catalytic Asp52 with an alanine residue increased the reaction rate of the promiscuous Mannich reaction. The proposed mechanism was also confirmed by molecular docking and molecular dynamic studies[28,29].

STAR★METHODS

Detailed methods are provided in the online version of this paper and include the following:

- KEY RESOURCES TABLE
- RESOURCE AVAILABILITY
  - Lead contact
  - Materials availability
  - Data and code availability
- METHOD DETAILS
  - General
  - HEWL activity and structure
  - Synthesis and characterization of biocomposites
  - HEWL mutation and expression
  - Computational study

SUPPLEMENTAL INFORMATION

Supplemental information can be found online at https://doi.org/10.1016/j.isci.2023.107807.

ACKNOWLEDGMENTS

AUTHOR CONTRIBUTIONS

DECLARATION OF INTERESTS

REFERENCES

1. Horváth, I.T., and Anastas, P.T. (2007). Innovations and green chemistry. Chem. Rev. *107*, 2169–2173. https://doi.org/10.1021/cr078380v.

2. Iles, A., and Mulvihill, M.J. (2012). Collaboration across disciplines for sustainability: Green chemistry as an emerging multistakeholder community. Environ. Sci. Technol. *46*, 5643–5649. https://doi.org/10.1021/es300803t.

3. Sheldon, R.A. (2012). Fundamentals of green chemistry: efficiency in reaction design. Chem. Soc. Rev. *41*, 1437–1451. https://doi.org/10.1039/C1CS15219J.

4. de Souza, R.O.M.A., Miranda, L.S.M., and Bornscheuer, U.T. (2017). A retrosynthesis approach for biocatalysis in organic synthesis. Chemistry (Basel). *23*, 12040–12063. https://doi.org/10.1002/chem.201702235.

5. Sheldon, R.A., and Brady, D. (2019). Broadening the scope of biocatalysis in sustainable organic synthesis. ChemSusChem *12*, 2859–2881. https://doi.org/10.1002/cssc.201900351.

6. Sheldon, R.A., and Pereira, P.C. (2017). Biocatalysis engineering: the big picture. Chem. Soc. Rev. *46*, 2678–2691. https://doi.org/10.1039/C6CS00854B.

7. Hult, K., and Berglund, P. (2007). Enzyme promiscuity: mechanism and applications. Trends Biotechnol. *25*, 231–238. https://doi.org/10.1016/j.tibtech.2007.03.002.

8. Bornscheuer, U.T., and Kazlauskas, R.J. (2004). Catalytic promiscuity in biocatalysis: using old enzymes to form new bonds and follow new pathways. Angew. Chem., Int. Ed. Engl. *43*, 6032–6040. https://doi.org/10.1002/anie.200460416.

9. Busto, E., Gotor-Fernández, V., and Gotor, V. (2010). Hydrolases: catalytically promiscuous enzymes for non-conventional reactions in organic synthesis. Chem. Soc. Rev. *39*, 4504–4523. https://doi.org/10.1039/C003811C.

10. Samsonowicz-Górski, J., Koszelewski, D., Kowalczyk, P., Śmigielski, P., Hrunyk, A., Kramkowski, K., Wypych, A., Szymczak, M., Lizut, R., Ostaszewski, R., and Ostaszewski, R. (2022). Promiscuous Lipase-Catalyzed Knoevenagel–Phospha–Michael Reaction for the Synthesis of Antimicrobial β-Phosphono Malonates. Int. J. Mol. Sci. *23*, 8819. https://doi.org/10.3390/ijms23158819.

11. Han, Y., Zhang, X., and Zheng, L. (2021). Engineering actively magnetic crosslinked inclusion bodies of Candida antarctica lipase B: An efficient and stable biocatalyst for enzyme-catalyzed reactions. Mol. Catal. *504*, 111467. https://doi.org/10.1016/j.mcat.2021.111467.

12. Bavandi, H., Habibi, Z., and Yousefi, M. (2020). Porcine pancreas lipase as a green catalyst for synthesis of bis-4-hydroxy coumarins. Bioorg. Chem. *103*, 104139. https://doi.org/10.1016/j.bioorg.2020.104139.

13. Lai, Y.F., Zheng, H., Chai, S.J., Zhang, P.F., and Chen, X.Z. (2010). Lipase-catalysed tandem Knoevenagel condensation and esterification with alcohol cosolvents. Green Chem. *12*, 1917–1918. https://doi.org/10.1039/C004547K.

14. He, Y.H., He, T., Guo, J.T., Li, R., Xiang, Y., Yang, D.C., and Guan, Z. (2016). Enzyme-catalyzed domino reaction: efficient construction of spirocyclic oxindole skeleton using porcine pepsin. Catal. Sci. Technol. *6*, 2239–2248. https://doi.org/10.1039/C5CY00987A.

15. Xie, Z.B., Wang, N., Zhou, L.H., Wan, F., He, T., Le, Z.G., and Yu, X.Q. (2013). Lipase-catalyzed stereoselective cross-aldol reaction promoted by water. ChemCatChem *5*, 1935–1940. https://doi.org/10.1002/cctc.201200890.

16. Xu, J.M., Zhang, F., Liu, B.K., Wu, Q., and Lin, X.F. (2007). Promiscuous zinc-dependent acylase-mediated carbon–carbon bond formation in organic media. Chem. Commun. 2078–2080. https://doi.org/10.1039/B700327G.

17. Xu, J.M., Zhang, F., Wu, Q., Zhang, Q.Y., and Lin, X.F. (2007). Hydrolase-catalyzed Michael addition of 1, 3-dicarbonyl compounds to α, β-unsaturated compounds in organic solvent. J. Mol. Catal. B Enzym. *49*, 50–54. https://doi.org/10.1016/j.molcatb.2007.08.004.

18. Liu, Z.Q., Xiang, Z.W., Shen, Z., Wu, Q., and Lin, X.F. (2014). Enzymatic enantioselective aldol reactions of isatin derivatives with cyclic ketones under solvent-free conditions. Biochimie *101*, 156–160. https://doi.org/10.1016/j.biochi.2014.01.006.

19. Li, H.H., He, Y.H., Yuan, Y., and Guan, Z. (2011). Nuclease p1: a new biocatalyst for direct asymmetric aldol reaction under solvent-free conditions. Green Chem. *13*, 185–189. https://doi.org/10.1039/C0GC00486C.

20. Li, C., Zhou, Y.J., Wang, N., Feng, X.W., Li, K., and Yu, X.Q. (2010). Promiscuous protease-catalyzed aldol reactions: A facile biocatalytic protocol for carbon–carbon bond formation in aqueous media. J. Biotechnol. *150*, 539–545. https://doi.org/10.1016/j.jbiotec.2010.10.004.

21. López-Iglesias, M., Busto, E., Gotor, V., and Gotor-Fernández, V. (2011). Use of Protease from Bacillus licheniformis as Promiscuous Catalyst for Organic Synthesis: Applications in C–C and C–N Bond Formation Reactions. Adv. Synth. Catal. *353*, 2345–2353. https://doi.org/10.1002/adsc.201100347.

22. Xue, Y., Li, L.P., He, Y.H., and Guan, Z. (2012). Protease-catalysed direct asymmetric Mannich reaction in organic solvent. Sci. Rep. *2*, 761–764. https://doi.org/10.1038/srep00761.

23. Guan, Z., Li, L.Y., and He, Y.H. (2015). Hydrolase-catalyzed asymmetric carbon–carbon bond formation in organic synthesis. RSC Adv. *5*, 16801–16814. https://doi.org/10.1039/C4RA11462K.

24. Li, C.J. (2005). Organic reactions in aqueous media with a focus on carbon− carbon bond formations: a decade update. Chem. Rev. *105*, 3095–3165. https://doi.org/10.1021/cr030009u.

25. Packer, M.S., and Liu, D.R. (2015). Methods for the directed evolution of proteins. Nat. Rev. Genet. *16*, 379–394. https://doi.org/10.1038/nrg3927.

26. Siegel, J.B., Zanghellini, A., Lovick, H.M., Kiss, G., Lambert, A.R., St Clair, J.L., Gallaher, J.L., Hilvert, D., Gelb, M.H., Stoddard, B.L., et al. (2010). Computational design of an enzyme catalyst for a stereoselective bimolecular Diels-Alder reaction. Science *329*, 309–313. https://doi.org/10.1126/science.1190239.

27. He, Y.H., Hu, W., and Guan, Z. (2012). Enzyme-catalyzed direct three-component aza-Diels–Alder reaction using hen egg white lysozyme. J. Org. Chem. *77*, 200–207. https://doi.org/10.1021/jo2016696.

28. Vocadlo, D.J., Davies, G.J., Laine, R., and Withers, S.G. (2001). Catalysis by hen egg-white lysozyme proceeds via a covalent intermediate. Nature *412*, 835–838. https://doi.org/10.1038/35090602.

29. Blake, C.C., Johnson, L.N., Mair, G.A., North, A.C., Phillips, D.C., and Sarma, V.R. (1967). Crystallographic studies of the activity of hen egg-white lysozyme. Proc. R. Soc. Lond. B Biol. Sci. *167*, 378–388. https://doi.org/10.1098/rspb.1967.0035.

30. Malcolm, B.A., Rosenberg, S., Corey, M.J., Allen, J.S., De Baetselier, A., and Kirsch, J.F. (1989). Site-directed mutagenesis of the catalytic residues Asp-52 and Glu-35 of chicken egg white lysozyme. Proc. Natl. Acad. Sci. USA *86*, 133–137. https://doi.org/10.1073/pnas.86.1.133.

31. Morris, D.L., Zampino, A.P., Taraboletti, A.A., Shriver, L.P., Leeper, T.C., and Ziegler, C.J. (2017). Lysozyme-catalyzed formation of a conjugated polyacetylene. Polym. Chem. *8*,

6344–6348. https://doi.org/10.1039/C7PY01250K.

32. Dalal, K.S., Wagh, Y.B., Tayade, Y.A., Dalal, D.S., and Chaudhari, B.L. (2018). Hen egg white lysozyme catalyzed efficient synthesis of 3-Indolyl-3-hydroxy Oxindole in aqueous ethanol. Catal. Lett. *148*, 3335–3341. https://doi.org/10.1007/s10562-018-2551-9.

33. Li, K., He, T., Li, C., Feng, X.W., Wang, N., and Yu, X.Q. (2009). Lipase-catalysed direct Mannich reaction in water: utilization of biocatalytic promiscuity for C–C bond formation in a "one-pot" synthesis. Green Chem. *11*, 777–779. https://doi.org/10.1039/B817524A.

34. Leonte, D., Bencze, L.C., Paizs, C., Irimie, F.D., and Zaharia, V. (2015). Heterocycles 38. Biocatalytic synthesis of new heterocyclic mannich bases and derivatives. Molecules *20*, 12300–12313. https://doi.org/10.3390/molecules200712300.

35. Guan, Z., Song, J., Xue, Y., Yang, D.C., and He, Y.H. (2015). Enzyme-catalyzed asymmetric Mannich reaction using acylase from Aspergillus melleus. J. Mol. Catal. B Enzym. *111*, 16–20. https://doi.org/10.1016/j.molcatb.2014.11.007.

36. Hong, X., Cholko, T., Chang, C.E.A., and Wheeldon, I. (2022). Multiscale simulation-guided design of enzyme bioconjugates with enhanced catalysis. Chem Catal. *2*, 2691–2703. https://doi.org/10.1016/j.checat.2022.09.018.

37. Ma, X., Sui, H., Yu, Q., Cui, J., and Hao, J. (2021). Silica Capsules Templated from Metal–Organic Frameworks for Enzyme Immobilization and Catalysis. Langmuir *37*, 3166–3172. https://doi.org/10.1021/acs.langmuir.1c00065.

38. Ly, H.G.T., Fu, G., de Azambuja, F., De Vos, D., and Parac-Vogt, T.N. (2020). Nanozymatic activity of UiO-66 metal–organic frameworks: tuning the nanopore environment enhances hydrolytic activity toward peptide bonds. ACS Appl. Nano Mater. *3*, 8931–8938. https://doi.org/10.1021/acsanm.0c01688.

39. Phipps, J., Chen, H., Donovan, C., Dominguez, D., Morgan, S., Weidman, B., Fan, C., Beyzavi, H., and Beyzavi, H. (2020). Catalytic activity, stability, and loading trends of alcohol dehydrogenase enzyme encapsulated in a metal–organic framework. ACS Appl. Mater. Interfaces *12*, 26084–26094. https://doi.org/10.1021/acsami.0c06964.

40. Zhang, Y., and Ma, S. (2021). Controllable immobilization of enzymes in metal-organic frameworks for biocatalysis. Chem Catal. *1*, 20–22. https://doi.org/10.1016/j.checat.2021.04.010.

41. Hu, H., Li, P., Wang, Z., Du, Y., Kuang, G., Feng, Y., Jia, S., Cui, J., and Cui, J. (2022). Glutamate oxidase-integrated biomimetic metal–organic framework hybrids as cascade nanozymes for ultrasensitive glutamate detection. J. Agric. Food Chem. *70*, 3785–3794. https://doi.org/10.1021/acs.jafc.2c01639.

42. Shen, X., Du, Y., Du, Z., Tang, X., Li, P., Cheng, J., Yan, R., Cui, J., and Cui, J. (2023). Construction of enzyme@ glutathione hybrid metal-organic frameworks: glutathione-boosted microenvironment fine-tuning of biomimetic immobilization for improving catalytic performance. Mater. Today Chem. *27*, 101326. https://doi.org/10.1016/j.mtchem.2022.101326.

43. Wang, Z., Liu, Y., Li, J., Meng, G., Zhu, D., Cui, J., and Jia, S. (2022). Efficient immobilization of enzymes on amino functionalized MIL-125-NH2 metal organic framework. Biotechnol. Bioproc. Eng. *27*, 135–144. https://doi.org/10.1007/s12257-020-0393-y.

44. Hosseini, S.R., Omidkhah, M., Mehri Lighvan, Z., Norouzbahari, S., and Ghadimi, A. (2023). Synthesis, characterization, and gas adsorption performance of an efficient hierarchical ZIF-11@ ZIF-8 core–shell metal–organic framework (MOF). Separ. Purif. Technol. *307*, 122679. https://doi.org/10.1016/j.seppur.2022.122679.

45. Gao, L., Chen, Q., Gong, T., Liu, J., and Li, C. (2019). Recent advancement of imidazolate framework (ZIF-8) based nanoformulations for synergistic tumor therapy. Nanoscale *11*, 21030–21045. https://doi.org/10.1039/C9NR06558J.

46. Ou, J., Yuan, X., Liu, Y., Zhang, P., Xu, W., and Tang, K. (2021). Lipase from pseudomonas cepacia immobilized into ZIF-8 as bio-catalyst for enantioselective hydrolysis and transesterification. Process Biochem. *102*, 132–140. https://doi.org/10.1016/j.procbio.2020.12.017.

47. Sun, Y., Shu, T., Ma, J., Dai, Q., Peng, P., Zhou, Z., Zhou, X., Su, L., Zhang, X., and Zhang, X. (2022). Rational design of ZIF-8 for constructing luminescent biosensors with glucose oxidase and AIE-type gold nanoclusters. Anal. Chem. *94*, 3408–3417. https://doi.org/10.1021/acs.analchem.1c05599.

48. Chi, J., Guo, M., Zhang, C., Zhang, Y., Ai, S., Hou, J., Wu, P., Li, X., and Li, X. (2020). Glucose oxidase and Au nanocluster co-encapsulated metal–organic frameworks as a sensitive colorimetric sensor for glucose based on a cascade reaction. New J. Chem. *44*, 13344–13349. https://doi.org/10.1039/C9NJ06339K.

49. Hoseinpour, V., and Shariatinia, Z. (2021). Applications of zeolitic imidazolate framework-8 (ZIF-8) in bone tissue engineering: A review. Tissue Cell *72*, 101588. https://doi.org/10.1016/j.tice.2021.101588.

50. Zhao, J., Li, H., Han, Y., Li, R., Ding, X., Feng, X., and Wang, B. (2015). Chirality from substitution: enantiomer separation via a modified metal–organic framework. J. Mater. Chem. A Mater. *3*, 12145–12148. https://doi.org/10.1039/C5TA00998G.

51. Guo, L., Liang, M., Wang, X., Kong, R., Chen, G., Xia, L., and Qu, F. (2020). The role of l-histidine as molecular tongs: a strategy of grasping Tb 3+ using ZIF-8 to design sensors for monitoring an anthrax biomarker on-the-spot. Chem. Sci. *11*, 2407–2413. https://doi.org/10.1039/D0SC00030B.

52. Wang, W., Zheng, S., Hong, Y., Xu, X., Feng, X., and Song, H. (2022). Hydrogel–Metal–Organic-Framework Nanoparticle Composites for Immobilization of Active Biomacromolecules. ACS Appl. Nano Mater. *5*, 2222–2230. https://doi.org/10.1021/acsanm.1c03904.

53. Paul, A., Vyas, G., Paul, P., and Srivastava, D.N. (2018). Gold-nanoparticle-encapsulated ZIF-8 for a mediator-free enzymatic glucose sensor by amperometry. ACS Appl. Nano Mater. *1*, 3600–3607. https://doi.org/10.1021/acsanm.8b00748.

54. Han, J., Huang, W., Zhao, M., Wu, J., Li, Y., Mao, Y., Wang, L., Wang, Y., and Wang, Y. (2021). A novel enhanced enrichment glucose oxidase@ ZIF-8 biomimetic strategy with 3-mercaptophenylboronic acid for highly efficient catalysis of glucose. Colloids Surf. B Biointerfaces *208*, 112034. https://doi.org/10.1016/j.colsurfb.2021.112034.

55. Kalhor, H.R., and Ashrafian, H. (2017). Identification of an aspidospermine derivative from borage extract as an anti-amyloid compound: a possible link between protein aggregation and antimalarial drugs. Phytochemistry *140*, 134–140. https://doi.org/10.1016/j.phytochem.2017.05.001.

56. Kalhor, H.R., Kamizi, M., Akbari, J., and Heydari, A. (2009). Inhibition of amyloid formation by ionic liquids: ionic liquids affecting intermediate oligomers. Biomacromolecules *10*, 2468–2475. https://doi.org/10.1021/bm900428q.

57. Zhang, Z., Li, J., Ji, M., Liu, Y., Wang, N., Zhang, X., Zhang, S., Ji, X., and Ji, X. (2021). Encapsulation of multiple enzymes in a metal–organic framework with enhanced electro-enzymatic reduction of CO 2 to methanol. Green Chem. *23*, 2362–2371. https://doi.org/10.1039/D1GC00241D.

58. Wu, H., Zhang, R., Zhang, W., Hong, J., Xiang, Y., and Xu, W. (2020). Rapid 3-dimensional shape determination of globular proteins by mobility capillary electrophoresis and native mass spectrometry. Chem. Sci. *11*, 4758–4765. https://doi.org/10.1039/D0SC01965H.

59. Liang, W., Ricco, R., Maddigan, N.K., Dickinson, R.P., Xu, H., Li, Q., Sumby, C.J., Bell, S.G., Falcaro, P., Doonan, C.J., and Doonan, C.J. (2018). Control of structure topology and spatial distribution of biomacromolecules in protein@ ZIF-8 biocomposites. Chem. Mater. *30*, 1069–1077. https://doi.org/10.1021/acs.chemmater.7b04977.

60. Maddigan, N.K., Linder-Patton, O.M., Falcaro, P., Sumby, C.J., Bell, S.G., and Doonan, C.J. (2021). Influence of the synthesis and storage conditions on the activity of Candida antarctica lipase B ZIF-8 biocomposites. ACS Appl. Mater. Interfaces *13*, 51867–51875. https://doi.org/10.1021/acsami.1c04785.

61. Xia, G.H., Cao, S.L., Xu, P., Li, X.H., Zhou, J., Zong, M.H., and Lou, W.Y. (2017). Preparation of a nanobiocatalyst by efficiently immobilizing Aspergillus niger lipase onto magnetic metal–biomolecule frameworks (BioMOF). ChemCatChem *9*, 1794–1800. https://doi.org/10.1002/cctc.201700070.

62. Ricco, R., Wied, P., Nidetzky, B., Amenitsch, H., and Falcaro, P. (2020). Magnetically responsive horseradish peroxidase@ ZIF-8 for biocatalysis. Chem. Commun. *56*, 5775–5778. https://doi.org/10.1039/C9CC09358C.

63. Li, Q., Chen, Y., Bai, S., Shao, X., Jiang, L., and Li, Q. (2020). Immobilized lipase in bio-based metal-organic frameworks constructed by biomimetic mineralization: A sustainable biocatalyst for biodiesel synthesis. Colloids Surf. B Biointerfaces *188*, 110812. https://doi.org/10.1016/j.colsurfb.2020.110812.

64. Yu, Y., Xu, N., Zhang, J., Wang, B., Xie, S., and Yuan, L. (2020). Chiral metal–organic framework d-His-ZIF-8@ SiO2 core–shell microspheres used for HPLC enantioseparations. ACS Appl. Mater. Interfaces *12*, 16903–16911. https://doi.org/10.1021/acsami.0c01023.

65. Lyu, F., Zhang, Y., Zare, R.N., Ge, J., and Liu, Z. (2014). One-pot synthesis of protein-embedded metal–organic frameworks with enhanced biological activities. Nano Lett. *14*, 5761–5765. https://doi.org/10.1021/nl5026419.

66. Feng, D., Liu, T.F., Su, J., Bosch, M., Wei, Z., Wan, W., Yuan, D., Chen, Y.P., Wang, X., Wang, K., et al. (2015). Stable metal-organic frameworks containing single-molecule traps

for enzyme encapsulation. Nat. Commun. *6*, 5979. https://doi.org/10.1038/ncomms6979.

67. Liu, G., Xu, Y., Han, Y., Wu, J., Xu, J., Meng, H., and Zhang, X. (2017). Immobilization of lysozyme proteins on a hierarchical zeolitic imidazolate framework (ZIF-8). Dalton Trans. *46*, 2114–2121. https://doi.org/10.1039/C6DT04582K.

68. Feng, Y., Hu, H., Wang, Z., Du, Y., Zhong, L., Zhang, C., Jiang, Y., Jia, S., Cui, J., and Cui, J. (2021). Three dimensional ordered magnetic macroporous metal-organic frameworks for enzyme immobilization. J. Colloid Interface Sci. *590*, 436–445. https://doi.org/10.1016/j.jcis.2021.01.078.

69. Hashimoto, Y., Yamada, K., Motoshima, H., Omura, T., Yamada, H., Yasukochi, T., Miki, T., Ueda, T., Imoto, T., and Imoto, T. (1996). A mutation study of catalytic residue Asp 52 in hen egg lysozyme. J. Biochem. *119*, 145–150. https://doi.org/10.1073/pnas.86.1.133.

70. Strynadka, N.C., and James, M.N. (1991). Lysozyme revisited: crystallographic evidence for distortion of an N-acetylmuramic acid residue bound in site D. J. Mol. Biol. *220*, 401–424. https://doi.org/10.1016/0022-2836(91)90021-W.

71. Ose, T., Kuroki, K., Matsushima, M., Maenaka, K., and Kumagai, I. (2009). Importance of the hydrogen bonding network including Asp52 for catalysis, as revealed by Asn59 mutant hen egg-white lysozymes. J. Biochem. *146*, 651–657. https://doi.org/10.1093/jb/mvp110.

72. Ding, Y.Q., Cui, Y.Z., and Li, T.D. (2015). New views on the reaction of primary amine and aldehyde from DFT study. J. Phys. Chem. A *119*, 4252–4260. https://doi.org/10.1021/acs.jpca.5b02186.

73. Chan, J.Y., Zhang, H., Nolvachai, Y., Hu, Y., Zhu, H., Forsyth, M., Gu, Q., Hoke, D.E., Zhang, X., Marriot, P.J., et al. (2018). Incorporation of homochirality into a zeolitic imidazolate framework membrane for efficient chiral separation. Angew. Chem. *130*, 17376–17380. https://doi.org/10.1002/ange.201810925.

74. Zhu, Q., Zhuang, W., Chen, Y., Wang, Z., Villacorta Hernandez, B., Wu, J., Yang, P., Liu, D., Zhu, C., Ying, H., et al. (2018). Nano-biocatalysts of Cyt c@ ZIF-8/GO composites with high recyclability via a de novo approach. ACS Appl. Mater. Interfaces *10*, 16066–16076. https://doi.org/10.1021/acsami.8b00072.

75. Asadi, V., Kardanpour, R., Tangestaninejad, S., Moghadam, M., Mirkhani, V., and Mohammadpoor-Baltork, I. (2019). Novel bovine carbonic anhydrase encapsulated in a metal–organic framework: a new platform for biomimetic sequestration of CO 2. RSC Adv. *9*, 28460–28469. https://doi.org/10.1039/C9RA04603H.

76. Wang, L., Zhi, W., Wan, J., Han, J., Li, C., and Wang, Y. (2019). Recyclable β-glucosidase by one-pot encapsulation with Cu-MOFs for enhanced hydrolysis of cellulose to glucose. ACS Sustain. Chem. Eng. *7*, 3339–3348. https://doi.org/10.1021/acssuschemeng.8b05489.

77. Lian, Z.X., Ma, Z.S., Wei, J., and Liu, H. (2012). Preparation and characterization of immobilized lysozyme and evaluation of its application in edible coatings. Process Biochem. *47*, 201–208. https://doi.org/10.1016/j.procbio.2011.10.031.

78. Wu, X., Yang, C., and Ge, J. (2017). Green synthesis of enzyme/metal-organic framework composites with high stability in protein denaturing solvents. Bioresour. Bioprocess. *4*, 24–28. https://doi.org/10.1186/s40643-017-0154-8.

79. Zheng, L., Baumann, U., and Reymond, J.L. (2004). An efficient one-step site-directed and site-saturation mutagenesis protocol. Nucleic Acids Res. *32*, e115. https://doi.org/10.1093/nar/gnh110.

80. Chang, A.Y., Chau, V., Landas, J.A., and Pang, Y. (2017). Preparation of calcium competent Escherichia coli and heat-shock transformation. JEMI methods *1*, 22–25.

81. Mine, S., Ueda, T., Hashimoto, Y., and Imoto, T. (1997). Improvement of the refolding yield and solubility of hen egg-white lysozyme by altering the Met residue attached to its N-terminus to Ser. Protein Eng. *10*, 1333–1338. https://doi.org/10.1093/protein/10.11.1333.

82. Laemmli, U.K. (1970). Cleavage of structural proteins during the assembly of the head of bacteriophage T4. nature *227*, 680–685. https://doi.org/10.1038/227680a0.

83. Ueda, T., Yamada, H., Aoki, H., and Imoto, T. (1990). Effect of chemical modifications of tryptophan residues on the folding of reduced hen egg-white lysozyme. J. Biochem. *108*, 886–892. https://doi.org/10.1093/oxfordjournals.jbchem.a123297.

84. Ibrahim, H.R., Higashiguchi, S., Koketsu, M., Juneja, L.R., Kim, M., Yamamoto, T., Sugimoto, Y., Aoki, T., and Aoki, T. (1996). Partially unfolded lysozyme at neutral pH agglutinates and kills Gram-negative and Gram-positive bacteria through membrane damage mechanism. J. Agric. Food Chem. *44*, 3799–3806. https://doi.org/10.1021/jf960133x.

85. Trott, O., and Olson, A.J. (2010). AutoDock Vina: improving the speed and accuracy of docking with a new scoring function, efficient optimization, and multithreading. J. Comput. Chem. *31*, 455–461. https://doi.org/10.1002/jcc.21334.

86. O'Boyle, N.M., Banck, M., James, C.A., Morley, C., Vandermeersch, T., and Hutchison, G.R. (2011). Open Babel: An open chemical toolbox. J. Cheminf. *3*, 1–14. https://doi.org/10.1186/1758-2946-3-33.

87. Morris, G.M., Huey, R., Lindstrom, W., Sanner, M.F., Belew, R.K., Goodsell, D.S., and Olson, A.J. (2009). AutoDock4 and AutoDockTools4: Automated docking with selective receptor flexibility. J. Comput. Chem. *30*, 2785–2791. https://doi.org/10.1002/jcc.21256.

88. Schüttelkopf, A.W., and van Aalten, D.M.F. (2004). PRODRG: a tool for high-throughput crystallography of protein–ligand complexes. Acta Crystallogr. D Biol. Crystallogr. *60*, 1355–1363. https://doi.org/10.1107/S0907444904011679.

STAR★METHODS

KEY RESOURCES TABLE

REAGENT or RESOURCE	SOURCE	IDENTIFIER
Bacterial strains		
Escherichia coli DE3	Iranian Biological Resource Center	ATCC 25922
Micrococcus luteus	School of Biology, University of Tehran, Iran	ATCC 4698
Chemicals, peptides, and recombinant proteins		
Zinc nitrate hexahydrate	Merck	CAS: 10196-18-6
2-Methylimidazole	Merck	CAS: 693-98-1
L-Histidine	Merck	CAS: 71-00-1
Polyvinylpyrrolidone	Merck	CAS: 9003-39-8
Aniline	Merck	CAS: 62-53-3
4-chloroaniline	Merck	CAS: 106-47-8
3-fluoroaniline	Merck	CAS: 372-19-0
Sec-butylamine	Merck	CAS: 13952-84-6
Methylamine	Merck	CAS: 74-89-5
Benzaldehyde	Merck	CAS: 100-52-7
4-methoxybenzaldehyde	Merck	CAS: 123-11-5
4-chlorobenzaldehyde	Merck	CAS: 104-88-1
2-chlorobenzaldehyde	Merck	CAS: 89-98-5
3-Nitrobenzaldehyde	Merck	CAS: 99 99-61-6
4-Hydroxybenzaldehyde	Merck	CAS: 123-08-0
Cyclohexanone	Merck	CAS: 108-94-1
Hen Egg White Lysozyme	BioBasic	Product Code: LDB0308
Mutant HEWL (D52A)	This work	N/A
Ampicillin	BioBasic	CAS: 69-52-3
Isopropyl β-D-1-thiogalactopyranoside	Sigma-Aldrich	CAS: 367-93-1
Oligonucleotides		
Upper: 5′-GACGGCTCGACCGCCTAT GGGATCTTA-3′	metabion	N/A
Lower: 5′-TAAGATCCCATAGGCGG TCGAGCCGTC-3′	metabion	N/A
Recombinant DNA		
Recombinant HEWL	Addgene	pET11a-4SS-HEWL
Mutated recombinant HEWL (D52A)	This work	N/A
Software and algorithms		
Origin 2018	Originlab	https://www.originlab.com/
AutoDock vina	Trott and Olson, 2010[85]	https://vina.scripps.edu/downloads/
Gromacs	Gromacs 5.1.2	http://www.gromacs.org

RESOURCE AVAILABILITY

Lead contact

Further information and requests for resources should be directed to the lead contact, Hamid R. Kalhor (kalhor@sharif.edu).

Materials availability

Experimental details have been found in the method details.

This study did not generate new unique reagents.

Data and code availability

- data reported in this paper will be shared by the lead contact upon request.
- This paper does not report original code.
- Any additional information required to reanalyze the data reported in this paper is available from the lead contact upon request. Hamid R. Kalhor (kalhor@sharif.edu).

METHOD DETAILS

General

All chemicals were purchased from Merck and used without any further purification. Hen egg white lysozyme (CAS RN: 12650-88-3) and ampicillin sodium salt USP were purchased from Bio Basic (Canada). Isopropyl β-D-1-thiogalactopyranoside (IPTG, >99% purity) was purchased from Sigma-Aldrich, respectively. NMR spectra were recorded at 500 MHz for proton and at 125 MHz for carbon nuclei on a Bruker (Avance DRX500) spectrometer in DMSO-d6 or CDCl$_3$ as solvents at room temperature. Chemical shifts are given in δ relative to tetramethylsilane (TMS). SEM image was achieved by utilizing Mira 3 scanning electron microscope. The infrared spectra were measured with a PerkinElmer Fourier Transform Infrared Spectrophotometer and are reported in wavenumbers using KBr discs (cm^{-1}). X-ray diffraction (PXRD) data were collected on an XPert Pro MPD (2–100 θ).

HEWL activity and structure

General procedure for the aldol addition, michael addition, and three-component mannich reaction catalyzed by HEWL

The Mannich reaction was initiated by adding 20 mg HEWL dissolved in deionized water (1mL) to a mixture of aldehyde (0.3 mmol), amine (0.33 mmol) and acetone (0.5 mmol) in a test tube containing a magnetic stirring bar. The suspension was stirred at 35°C for 9 h and the progress of the reaction was monitored by thin-layer chromatography (TLC). After completion of the reaction, HEWL was precipitated by adding four times the sample volume of acetone to the reaction mixture, and the solution was then filtered off. The organic layer was dried over Na$_2$SO$_4$ and the organic solvent was removed in vacuo. The crude product was purified by preparative thin-layer chromatography (PTLC) from Merck silica gel 60 PF$_{252}$ on 20*20 plates using a mixture of n-hexane/EtOAc (3:1) as eluent. The desired β-amino carbonyl products were gained in 50–82% yields (Table 2). To perform the aldol reaction a mixture of 3-nitrobenzaldehyde (0.2 mmol), cyclohexanone (0.1 mmol), and HEWL (10 mg) in deionized water (1 mL) was stirred at 35°C for 20 h. The reaction progress was monitored by TLC. Michael addition was carried out in a test tube containing cyclohexanone (0.1 mmol) and HEWL (10 mg) in deionized water (1 mL) while 2-cyclohexenone (0.1 mmol) was slowly added to the mixture. The resulting mixture was stirred at 35°C for 20 h and the reaction was monitored by TLC. An alternative Mannich reaction comprising cyclohexanone (0.5 mmol), aldehyde (0.3 mmol), and amine (0.33 mmol) was successively added to a solution of HEWL (20 mg) in deionized water (1 mL) placed in a test tube and stirred at 35°C for about 16 h. After completion, the reaction was quenched by adding 4 times the sample volume of acetone to the reaction mixture and filtering off the enzyme. The filtrate was dried with Na$_2$SO$_4$ and then concentrated under reduced pressure to afford the crude product. The residual crude product was purified by preparative thin-layer chromatography and crystallized from ethanol.

Acetone precipitation of HEWL

For separating the enzyme from the reaction mixture, four times the sample volume of acetone was pre-cooled at 20°C and added slowly to the reaction mixture. The resulting mixture, was then incubated at 0°C–4°C and after 2 h the suspension was centrifuged and precipitant was filtered off the supernatant.

Circular dichroism (CD) spectropolarimetry

CD spectra of recycled HEWL for 4 consecutive runs were recorded at a final concentration of 0.2 mg/mL from 190 to 260 nm (far-UV) using 1 mm path quartz cell at room temperature. Experiments were performed on a 215 Aviv spectropolarimeter (USA); the baseline was corrected with deionized water. The percentages of secondary structure elements (helix, β-sheet, β-turn, and loop) were predicted using CDNN 2.1 software.

Intrinsic fluorescence measurements

Fluorescence of Recycled HEWL samples with a concentration of 0.125 mg/mL was measured after exciting at 295 nm and recording the emission from 300 to 400 nm using Fl-win lab photomultiplier LS 50 (PerkinElmer) spectrofluorometer. This experiment was used to investigate Trp intrinsic fluorescence.

Bacterial strains and plasmids

The gene encoding hen egg white lysozyme in an expression vector pET11a with an N-terminal methionine was used. *E. coli* DH5α and BL21 (DE3) were used as host cells in DNA manipulation. *Micrococcus luteus* ATCC 4698 was obtained from the School of Biology, University of Tehran.

Turbidimetric lysozyme assay

The lysis of Gram-positive bacteria *Micrococcus luteus* (*Micrococcus lysodeikticus*) was determined based on the turbidimetric method. A suspension of *M. luteus* (0.25 mg/mL) in 1.9 mL 0.05 M phosphate buffer at pH 7.0 was prepared and 100 μL of renatured lysozyme was transferred to the aforementioned buffer and then a decrease in absorbance was measured every 2 min for a total time period of 20 min and 10-min intervals for the next 40 min at 450 nm using UNICO 2150-UV spectrophotometer. The reaction was carried out at 25°C.

Characterization of the Mannich products

4-(4-methoxyphenyl)-4-(phenylamino)butan-2-one (β1). White solid; 1H NMR (500 MHz, DMSO-d6): δ 7.3(d, J = 8.7, 2H), 6.9(t, J = 7.5, 2H), 6.8(d, J = 8.7, 2H), 6.5(d, J = 8.45, 2H), 6.45(t, J = 7.25, 1H), 6.1 (br, 1H), 4.75 (m, 1H), 3.69 (s, 3H), 2.77 (dd, 2H), 2.1 (s, 3H) ppm; 13C NMR (125 MHz, DMSO-d6): δ 206.74, 158.47, 148.23, 136.11, 129.13, 127.99,116.3, 114.13, 113.42, 55.41, 52.64, 51.89, 30.53 ppm; The enantiomeric excess was determined by HPLC (Daicel Chiralpak AD-H, hexane/isopropanol = 85:15, flow rate 0.8 mL/min, λ = 254 nm), tR = 10.800 (minor), 13.767 (major).

4-(3-nitrophenyl)-4-(phenylamino)butan-2-one (β2). Yellow solid; 1H NMR (500 MHz, DMSO-d6): δ 8.32 (s, 1H), 8.05(d, J = 8.15, 1H), 7.89(d, J = 7.6, 1H), 7.60(t, J = 7.85, 1H), 7.02(t, J = 7.4, 2H), 6.56(d, J = 8.5, 2H), 6.50(t, J = 7.95, 1H), 6.36 (br, 1H), 5.02 (m,1H), 2.87 (dd, 2H) 2.14 (s, 1H) ppm; 13C NMR (125 MHz, DMSO-d6) δ: 198.59, 148.79, 141.09, 136.88, 134.56, 130.91, 130.11, 125.05, 123.49, 60.60, 47.99, 28.02 ppm.

4-(2-chlorophenyl)-4-(phenylamino)butan-2-one (β3). White solid; 1H NMR (500 MHz, CDCl3): δ 7.48 (m, 1H), 7.46 (m, 1H), 7.29 (m, 2H), 7.12(t, J = 7.8, 2H), 6.71(t, J = 7.15, 1H), 6.51(d, J = 8.15, 2H), 5.23 (m, 1H), 4.72 (s, 1H), 3.04 (dd, 2H), 2.20 (s, 3H) ppm; 13C NMR (125 MHz, CDCl3) δ: 207.34, 146.30, 139.09, 132.36, 129.86, 129.17, 128.57, 127.78, 127.42, 118.03, 113.57, 51.56, 48.92, 30.17 ppm; The enantiomeric excess was determined by HPLC (Daicel Chiralpak AD-H, hexane/isopropanol = 90:10, flow rate 1 mL/min, λ = 254 nm), tR = 8.850 (minor), 9.917 (major).

4-(4-chlorophenyl)-4-(phenylamino)butan-2-one (β4). Yellow solid; 1H NMR (500 MHz, DMSO-d6): δ 7.49(d, J = 8.45, 2H), 7.35(d, J = 8.45, 2H), 7.00(t, J = 8.25, 2H), 6.51 (d, J = 7.85, 2H), 6.47(t, J = 6.7, 1H), 6.2 (br, 1H), 4.86 (m, 1H), 2.93 (dd, 1H), 2.76 (dd, 1H), 2.12 (s, 3H) ppm; 13C NMR (125 MHz, DMSO-d6): δ 206.36, 147.97, 143.44, 131.61, 129.21, 128.89, 128.70, 116.56, 113.39, 52.53, 51.48, 30.46 ppm.

4-Phenyl-4-(phenylamino)butan-2-one (β5). White solid; 1H NMR (500 MHz, CDCl3): δ 7.41(d, J = 7.6, 2H), 7.35(t, J = 7.3, 2H), 7.27(d, J = 9.1, 1H), 7.13(t, J = 7.6, 2H), 6.72(t, J = 6.85, 1H), 6.59(d, J = 8.3, 2H), 4.88(t, J = 6.5, 1H), 2.96(d, J = 6.5, 2H), 2.11 (s, 3H) ppm; 13C NMR (125 MHz, CDCl3): δ 206.79, 146.96, 142.33, 129.13, 128.80, 127.35, 126.26, 117.92, 113.76, 52.52, 51.29, 30.73 ppm; The enantiomeric excess was determined by HPLC (Daicel Chiralpak AD-H, hexane/isopropanol = 90:10, flow rate 1 mL/min, λ = 254 nm), tR = 13.100 (minor), 15.300 (major).

4-(sec-butylamino)-4-phenylbutan-2-one (β6). Yellow solid; 1H NMR (500 MHz, DMSO-d6): δ 7.38 (m, 4H), 7.23 (dd, 1H), 5.84 (br, 1H), 2.65 (m, 3H), 2.46 (m, 2H), 2.13(d, J = 8, 1H), 1.99 (s, 3H), 1.62 (s, 1H), 1.24 (s, 3H), 0.88(d, J = , 1H) ppm; 13C NMR (125 MHz, DMSO-d6): δ 198.40, 128.93, 127.34, 127.03, 125.93,55.78, 43.95, 38.59, 24.32, 9.28 ppm; The enantiomeric excess was determined by HPLC (Daicel Chiralpak AD-H, hexane/isopropanol = 90:10, flow rate 1 mL/min, λ = 254 nm), tR = 10.483 (minor), 10.900 (major).

4-((3-fluorophenyl)amino)-4-phenylbutan-2-one (β7). Yellow solid; 1H NMR (500 MHz, DMSO-d6): δ 7.40 (d, J = 7.5, 2H), 7.30 (t, J = 7.65, 2H), 7.21 (t, J = 7.3, 1H), 6.99 (q, J = 7.8, 1H), 6.55 (d, J = 7.75, 1H), 6.35 (d, J = 7.65, 1H), 6.22 (t, J = 8.15, 1H), 2.90 (dd, 2H), 2.12 (s, 3H) ppm; 13C NMR (125 MHz, DMSO-d6): δ 207.52, 150.10, 143.57, 130.62, 129.51, 128.93, 128.82, 127.45, 126.78, 110.58, 109.62, 53.08, 51.31, 30.51 ppm.

4-((4-chlorophenyl)amino)-4-phenylbutan-2-one (β8). Yellow solid; 1H NMR (500 MHz, DMSO-d6): δ 7.37 (d, J = 7.05, 2H), 7.30 (t, J = 7, 2H), 7.20 (t, J = 6.9, 1H), 7.01 (d,J = 7.95, 2H), 6.52 (d, J = 7.95, 2H), 6.38 (br,1H), 4.80 (m, 1H), 2.85 (dd, 2H), 2.12 (s,3H) ppm; 13C NMR (125 MHz, DMSO-d6): δ 199.37, 143.89, 128.87, 128.82, 126.87, 119.22, 114.68, 107.89, 105.89, 53.21, 51.65, 30.06 ppm.

4-(methylamino)-4-phenylbutan-2-one (β9). Colorless solid; 1H NMR (500 MHz, DMSO-d6): δ 7.27 (t, J = 7.27, 2H), 6.99 (t, J = 6.9, 3H), 6.36 (m, 1H), 2.86 (s, 2H), 2.06 (s, 1H), 1.90 (s, 1H), 0.79 (s, 1H) ppm; 13C NMR (125 MHz, DMSO-d6): δ 191.81, 130.45, 128.96, 128.85, 128.39, 50.20, 42.39, 33.64, 27.35 ppm.

2-((4-hydroxyphenyl)(phenylamino)methyl)cyclohexan-1-one (β10). Yellow solid; Colorless solid; 1H NMR (500 MHz, DMSO-d6): δ 9.69 (s, 1H), 7.67 (d, J = 8.5, 2H), 7.36 (d, J = 3.45, 2H), 7.31 (s, 1H), 6.82 (d, J = 8.5, 2H), 6.78 (d, J = 8.2, 2H) 2.77 (m, 2H), 2.41 (t, J = , 2H), 1.83 (m, 3H), 1.70 (m, 3H) ppm.

2-((2-chlorophenyl)(phenylamino)methyl)cyclohexan-1-one (β11). Yellow solid; 1H NMR (500 MHz, CDCl3): δ 7.58 (d, J = 7.5, 1H), 7.35 (d, J = 7.35, 1H), 7.28 (s, 1H), 7.18 (t, J = 7.19, 1H), 7.15 (d, J = 7.16, 1H), 7.10 (t, J = 7.1, 1H), 6.65 (t, J = 6.65, 1H), 6.52 (d, J = 6.5, 1H), 4.91 (d, J = 4.9, 1H), 2.95 (m, 1H), 2.38 (m, 2H), 2.10 (m, 4H), 1.79 (m, 2H) ppm; 13C NMR (125 MHz, CDCl3): δ 212.99, 133.33, 129.29, 129.21, 128.98, 128.23, 127.07, 117.52, 113.34, 55.37, 43.46, 42.86, 32.70, 28.12, 24.81 ppm.

2-((4-methoxyphenyl)(phenylamino)methyl)cyclohexan-1-one (β12). Yellow solid; 1H NMR (500 MHz, DMSO-d6): δ 7.52 (t, J = 8.7, 1H), 7.47 (d, J = 8.7, 1H), 7.42 (d, J = 8.75, 2H), 7.37 (d, J = 8.7, 1H), 6.95 (t, J = 8.8, 3H), 6.83 (d, J = 8.8, 1H), 3.86 (s, 3H), 2.95 (m, 1H), 2.87 (m, 2H), 2.62 (m, 1H), 2.52 (m, 2H), 1.94 (m, 4H), 1.81 (m, 2H) ppm; 13C NMR (125 MHz, CDCl3): δ 214.15, 159.93, 135.8, 134.44, 132.26, 131.43, 130.48, 113.86, 113.52, 55.31, 40.16, 28.99, 26.55, 23.85, 23.28 ppm; The enantiomeric excess was determined by HPLC (Daicel Chiralpak AD-H, hexane/iso-propanol = 80:20, flow rate 1 mL/min, λ = 254 nm), tR = 4.533 (minor), 27.217 (major).

Synthesis and characterization of biocomposites

Preparation of ZIF-8 nanocrystals

ZIF-8 nanocrystals were synthesized according to reporting literature.[59] Briefly, a solution of $Zn(NO_3)_2.6H_2O$ (1.2 mmol) in 20 mL water was added dropwise into a solution of 2-methylimidazole (4.8 mmol) in 20 mL water under stirring. After stirring at room temperature for 24 h, ZIF-8 was formed, then separated by centrifugation at 13000 rpm for 3 min and washed with water three times. The collected white powder was dried in the oven at 60°C overnight.

Synthesis of HEWL-His/ZIF-8 crystals

1.2 mmol L-His was dissolved in 16 mL deionized water. 250 μL of triethyl amine (TEA) was then added into the His solution and stirred for 5 min 2.4 mmol $Zn(NO_3)_2.6H_2O$ and 8.4 mmol 2-methylimidazole (2-mIM) were dissolved in 40 mL and 24 mL water, respectively. To prepare the ZIF-8 precursor solution, 2-mIM solution was first mixed and stirred with His solution for 15 min (solution A), and 40 mg of HEWL (1 mg/mL) was added to $Zn(NO_3)_2.6H_2O$ solution (solution B), followed solution B was added dropwise to the solution A. The solution was stirred for 24 h. The product was collected by centrifugation at 13000 rpm for 3 min and repeatedly washed 3 times to remove the adsorbed protein. The collected white powder was dried at room temperature and kept at 4°C in the refrigerator.[73]

Synthesis of PVP-modified HEWL encapsulated in ZIF-8

1.2 mmol L-His was dissolved in 16 mL deionized water. 250 μL of TEA was then added into the His solution and stirred for 5 min 8.4 mmol 2-mIM was dissolved in 24 mL water and stirred with His solution for 15 min (solution A). 2.4 mmol $Zn(NO_3)_2.6H_2O$ was dissolved in 40 mL water, subsequently, 500 μL from HEWL solution (50 mg HEWL in 15 mg/mL water solution of Polyvinylpyrrolidone (PVP) as started with Zheng Liu and his coworkers in 2014 and repeated in 2018 by Zhonghua Zhu research group[65,74]) was added to zinc nitrate solution (solution C). Eventually, solution C was added dropwise to the solution A. The solution was stirred for 24 h. The product was collected by centrifugation at 13000 rpm for 3 min and repeatedly washed 3 times to remove the adsorbed protein. The collected white powder was dried at room temperature and kept in 4°C in the refrigerator.

Thermal gravimetric analysis (TGA)

TGA was performed using Mettler Toledo (TGA-DSC 1) as thermal gravimetric analyzer with a heating rate of 20°C/min from 40°C to 600°C under nitrogen environment with a flow rate of 50 mL/min[75]

Immobilization efficiencies of enzymes in ZIF-8 and maximum loading

Encapsulation efficiency factor, which measures the ratio of the enzyme content embedded in the biocomposite to the initial amount of enzyme (Equation 1), was used to quantify the enzyme concentration that was encapsulated in ZIF-8.

$$Encapsulation\ efficiency\ (\%) = ((m - CV)\ /\ m)100 \qquad \text{(Equation 1)}$$

By measuring the initial enzyme amount (m (mg)), volume of supernatant (V (mL)), and enzyme concentration in supernatant (C (mg/mL)) using a standard Bradford Assay.[76]

The maximum loading was achieved by different concentration of HEWL from 0.05 to 5 mg/mL, reaching saturated loading of enzyme in ZIF-8 within 24 h. The PHHZ with different concentrations of HEWL was synthesized as described above in "synthesis of PVP-modified HEWL encapsulated in ZIF-8", after separating the PHHZ from the solution, the concentration of the HEWL in the solution was measured using UV-Vis spectrophotometer, and then the concentrated of enzyme loaded in the ZIF-8 was calculated. The maximum loading was calculated based on the milligram of encapsulated enzyme per milligram of ZIF-8 produced.

Kinetic analysis

The maximal velocity (V_{max}) and the Michaelis constant (K_m) were estimated for the free-HEWL and immobilized-HEWL (PHHZ) with lyophilized *Micrococcus lysodeikticus* (0.02–0.5 mg/mL) as substrate in 10 min. Assays were carried out in triplicate and lytic activity was measured as the decrease in turbidity at OD_{450} nm using UNICO 2150-UV spectrophotometer. Lineweaver-Burk plots was used for the experimental data calculation.[77]

Determining the amount of enzyme encapsulated in the ZIF-8

20 mg of PHHZ was weighted and after further washing with water, it was digested with acetic acid, then the enzyme loading amount was measured by Bradford assay at 595 nm using UNICO 2150-UV spectrophotometer.[78]

HEWL mutation and expression

Site-directed mutagenesis and construction of HEWL mutant proteins

Site-directed mutagenesis was carried out according to the method of Lei Zheng (2004).[79] one 27-base synthetic primer (see Table S6) was used in separate experiments to alter the catalytic aspartic acid 52 to alanine. The nucleotide sequence of the mutant protein was confirmed by DNA sequencing (see Figure S44). The expression plasmids of the wild-type and mutant lysozyme were termed pET11a-Wt and pET11a-D52A; the linear plasmid map of the pET11a-4SS-HEWL (Addgene) has shown in Figure S45. Agarose gel electrophoresis of native and mutant lysozyme have shown in Figures S46A and S46B, respectively.

Expression of mutant lysozyme in E. Coli

The expression vectors were transformed into BL21 (DE3) competent cells according to the calcium chloride method.[80] A single colony from the transformation plate was inoculated in 5 mL of LB broth medium containing 100 μg/mL ampicillin (filter-sterilized) and was shaken at 200 rpm for 16 h at 37°C. cultures were induced with 1 mM IPTG at an OD_{600} of about 0.4–0.8 and grown for an additional 3 h before harvesting. The cell lysate was prepared by an ultrasonic pulse (TOPSONICS, UP-2000) in buffer containing 50 mM Na_3PO_4, 300 mM NaCl, 10 mM imidazole, 0.5% tween 20, pH 8 for 10 s 40 times in an ice-water bath. Cell lysates were then centrifuged at 8000 g for 10 min. The resulting pellets (inclusion bodies) were solubilized in 8 M urea. To confirm the overproduction of the desired enzyme SDS-PAGE analysis was carried out. Renaturation of inactive hen egg white lysozyme was performed according to the method of Mine, S (1997).[81]

Sodium dodecyl sulfate-polyacrylamide gel electrophoresis (SDS-PAGE)

SDS-PAGE was performed under reducing condition (5% β-mercaptoethanol) using a 4% acrylamide stacking gel and 20% separating gel containing 2% SDS, 0.01 bromophenol blue, 60 mM Tris-HCl (pH 6.8) and 10% glycerol in slab gels and stained with Coomassie brilliant blue R-250 (CBB) according to the method of Laemmli.[82] The SDS-PAGE analysis of wild-type and D52A lysozyme has shown in Figures S47A and S47B, respectively.

Renaturation of reduced hen egg-white lysozyme

Renaturation of reduced hen egg white lysozyme both native and mutants was performed as stated by Ueda (1990)[83] and slight modification was reported by Mine, S (1997). Denatured HEWL pellets were dissolved in 500 μL of 8 M urea and to prepare the solution for subsequent reduction, the mixture was degassed. 5 μL of β-mercaptoethanol was added to the solution and then the solution was incubated at 40°C for 2 h under a nitrogen atmosphere (reduced solution). 16.2 mg of oxidized glutathione (GSSG) dissolved in 100 μL of 8 M urea was added to the reduced solution (redox solution). At the same time, 19.8 mL of the 0.1 M Tris–HCl buffer containing 1 mM EDTA pH 8.0 and 0.695 mM GSSG was preincubated at 40°C (renaturation buffer). Renaturation of the reduced hen egg-white lysozyme was initiated by adding 200 μL of redox solution to the renaturation buffer while the solution was stirred. The recovery of the lytic activity was monitored according to the literature (Ibrahim 1996).[84] The decrease in turbidity of 1.9 mL of *M.luteus* cell suspension (0.25 mg/mL) in 50 mM sodium phosphate buffer (pH 6.2) following the addition of 100 μL of renaturation mixture was measured at 450 nm.

Computational study

Molecular docking studies

AutoDock Vina (Trott and Olson, 2010)[85] was used in this study. Illustrations generated using PyMOL and OpenBabel (O'Boyle et al., 2011)[86] as molecular format conversion software was employed to prepare ligand for docking. Receptor preparation and defining the optimal grid box were achieved using AutoDock Tools version 1.5.6. (Morris et al., 2009).[87] PRODRG 2.x online server was used to create energy minimized 3D structure of ligands.[88] The crystal structure of HEWL was retrieved from RCSB Protein DataBank (PDB: 2EPE). All water molecules were removed from the crystal structure. The AutoDock-base blind docking approach was employed to search the entire protein surface. The missing hydrogen atoms were added to the receptor file and after the addition of charges to ligand and receptor PDB files, the PDBQT format was generated for both input files. The grid sizes along the X, Y, and Z axes were fixed to 92 90 116 with a spacing of 0.375 Å and the grid box was centered at the coordinates of x 2.015, y 57.252 and z 0.433 of the crystal structure of HEWL. The docking analysis was conducted by AutoDock Vina.

MD simulations

At a physiological pH of 7.4, the GROMOS87/GROMOS96 force field has been used for all simulations. Each system was situated in the middle of a cubic box that was at least 1.0 nm away from the center. The box containing protein was solvated with pre-equilibrated SPC water molecules, and sufficient number of Cl^- or Na^+ ions were replaced to water molecules to neutralize the system. Energy was minimized using 100 PS equilibration in the constant-volume, constant temperature ensemble (NVT) and the constant-pressure, constant temerature ensemble (NPT) with temperature and pressure coupling set to 300 K and 1.0 bar, respectively, using the steepest descent integrator with an emtol value of 10 kJ/(mol nm). For each system, an unrestricted MD simulation was performed at 300 K. Energy, coordinates, and velocities were stored every 1.0 ps for equilibrations and 10.0 ps for MD in all steps with an integration time of 2 fs. The cutoff value for both equilibration and MD was set to 1.2 nm, and all bonds were constrained using the Lincs algorithm61 and van der Waals interactions using a Verlet cutoff method updated every 20 fs. For long-range electrostatics, a Fourier spacing value of 0.16 was utilized with the PME method56. Parrinello-Rahman55 and V-rescale62 methods were used for the coupling of pressure and temperature, respectively. MD simulations were run for 10 ns in total.